STUDIES ON METAL-ORGANIC INTERACTIONS FOR CHEMICAL SPECIATION IN MODEL SYSTEMS

M.PHIL THESIS

SUBMITTED BY

SILVIA KHAIR

REGISTRATION NO.283

SESSION: 1996-97

A Thesis submitted to the Department of Chemistry, University of Dhaka,
in partial fulfillment of the requirements for the degree of
Master of Philosophy

Inorganic and Analytical Laboratory
Department of Chemistry
University of Dhaka, Dhaka 1000,
December, 2008

Certificate

This is to certify that the thesis titled "Studies on metal Organic Interactions for chemical speciation in model systems" Submitted by Silvia Khair of registration no. 283, Session 1996-97 for the degree of Master of Philosophy, University of Dhaka, is a record of original research work. Silvia Khair has carried out this research work under our supervision and guidance at the Department of Chemistry, University of Dhaka. The Result used in this thesis has not been used or submitted elsewhere for the award of any other degree.

This thesis is worthy for the award of the degree of "Master of Philosophy" in accordance with the rules and regulation of Dhaka University.

Supervisors:

27/12/08

1. **Professor (Rtd.) A.H.Khan**
   Department of Chemistry
   University of Dhaka.

27.12.08

2. **Professor P.K. Bakshi**
   Department of Chemistry
   University of Dhaka.

Acknowledgements

I would like to express my deepest gratitude to my supervisors Professors Dr. Amir H. Khan and Dr. Pradip K. Bakshi, Department of Chemistry, University of Dhaka, for their unparallel inspiration and constant guidance on my topic of interest.

I would like to express my gratefulness to Professor Dr. Tajmeri S. A Islam, Chairperson, Department of Chemistry, University of Dhaka, for giving me an opportunity to work as an M. Phil. student.

I am also thankful to Professor Shafiqul Alam and all the teachers of Department of Chemistry, University of Dhaka, for their guidance and suggestions during my entire research works.

I am grateful to Assistant Professor Dr. Abdul Jabbar, Department of Chemistry, University of Dhaka, for his assistance on various occasions especially during writing of this thesis.

I am grateful and indebted to my parents for their love, support motivation and assistance during the course of this work.

I express my sense of gratitude to my husband Md. Abu Shah Jalal Azad, my brother, sister, my son Sharaf, father-in-law, mother-in-law and all my relatives who have provided supports, inspiration and stood by me throughout the time to carry out this research work successfully.

I am highly indebted to Dr. Shaila Salauddin for her assistance on countless occasions during working in this project and make my life easier to survive in this field.

I am grateful to my colleagues in the Khan's research group, Mr. Shahed Reza, Mr. Abdul Halim, for their assistance on countless occasions, and to my friends and family for their ongoing support.

The cooperation of Prof. Alam's group is highly appreciated. Dr. Arifur Rahman, Mr. Siddique, Mrs. Ferhana Ferdousie, Mr. Shadequr Rashid Roni are all friendly, helpful and full of good ideas.

The efforts of the technical and support staff are also acknowledged, as are those of Mr. Halimur Rahman for UV-VIS, and Mr. Ashish for various assistance.

Silvia Khair
Department of Chemistry
University of Dhaka.

TABLE OF CONTENTS

List of Figures

List of Tables

Abstract

Interaction of divalent metal ions such as Cu(II) and Cd(II) with catechol has been studied using cyclic voltammetric technique at glassy carbon electrode (GCE). Cyclic volatammograms (CVs) of free metal ions, catechol and the metal ions in the presence of catechol are recorded in 0.5 M KCl solution and in the buffer solution of pH 4.23. 1:1, 1:2 and 1:3 metal to catechol molar ratios and various scan rates are also used in this investigation.

Two steps, each of one-electron transfer processes are observed in the CV of copper, of which the Cu(II)/Cu(I) couple is reversible and the Cu(I)/Cu(0) is quasi-reversible. However, in the presence of catechol, both anodic and cathodic peaks are shifted towards more cathodic region, which demonstrates the formation of complex between copper and catechol in solution. Higher the positive charge on the copper ion, stronger is its tendency to interaction with catechol. The nature of voltammograms at different metal to catechol ratios also supports this observation.

In cyclic voltammetric studies of cadmium system, simultaneous two electron transfer process is observed in CV, of which the Cd(II)/Cd(0) couple is reversible. In presence of catechol, shifting of both anodic and cathodic peaks occurs possibly due to the formation of complex between cadmium and catechol under the present experimental condition. Gradual decrease of cathodic current with the increase of catechol concentration also demonstrates the cadmium-catechol interaction. Cadmium with 2^+ charge and high concentration of catechol favors the complex formation reaction.

Spectroscopic investigation in the ultra-violet region has also been performed. The continuous variation method of a series of solutions of (Cu(II), and Cd(II) added to catechol having different molar ratios shows that they interact with each other and form complex. Jobs-plots from the spectroscopic data enable the empirical formula of the complex ions that formed in the solution phase.

Glossary of Symbols

δ	Chemical shift
$\Delta^{\nu_{1/2}}$	Bandwidth at half intensity
ϵ_{max}	Extinction coefficient maximum
μ	Charge carrier mobility
ν	Scan speed
ν_{max}	Absorption maximum wave number
σ	Conductivity
ω	Impedance frequency
A	Electrode surface area
C_{low}	Low frequency capacitance
C_F	Faradaic capacitance
C_g	Geometric capacitance
C_x	Concentration of x
D_{CT}	Charge transport diffusion coefficient
D_e	Electron diffusion coefficient
D	Film thickness
$E_{1/2}$	Half-wave potential
E_g	Band gap
E_{op}	Optical electron transfer barrier
E_p	Peak potential
E_{pa}	Anodic peak potential
E_{pc}	Cathodic peak potential
E_{th}	Thermal electron transfer barrier
F	Faraday's constant
I	Current
J	Current density
M	mol/L
N	Number of charge carriers
N	Number of electrons
R	Gas constant

R_{Σ}	Total resistance ($R_i + R_c$)
R_c	Electronic resistance
R_i	Ionic resistance
S	Standard deviation

Chapter I

1. Introduction

1.1 Chemical Speciation

Chemical speciation is concerned with identification and quantification of specific forms of an element[1] and its complexes in solution. As different chemical forms of an element may exhibit differing degrees of toxicities and mobilities in the environment, it is clearly of importance to be able to distinguish between the individual species present in a particular sample.

Metal speciation and bioavailability in aquatic systems is invaluable for chemists, biochemists, biologists, ecologists and environmental engineers because it provides:

(i) A comprehensive approach to the subject covering all aspects of trace metal ecotoxicology in the environment.

(ii) An introduction to the use of laboratory bioassays as predictive tools for understanding trace metal-organism interactions.

(iii) An examination of the use and limitations of bioassays in management decisions.

The legal release and disposal of copper or copper-laden effluents into estuarine waters poses a serious environmental, engineering and economic challenge to the navy and the country in general. This is because EPA-mandated Water Quality Criteria (WQC) for copper effluents are at or very close to the ambient or "normal" concentrations of copper in many estuaries, which are at the low μg/L level[2]. The issue is, in fact, scientifically complex because effluents are dispersed, copper is complexed and rendered less toxic by natural organic matter, and because of the ability of organisms to adapt and fill niches vacated by more sensitive species. There is evidence in the literature that the ratio of free copper to total dissolved copper ($Cu(II)_{aq}/Cu_{Total}$) may vary both temporally and spatially due to local mixing processes, adsorption on particulates and the ability of marine microorganisms to produce copper-sequestering materials. Therefore, in order to better relate WQC to natural conditions, a concerted effort should be made to understand how $Cu(II)_{aq}/Cu_{Total}$ changes in the natural environment as well as during toxicity tests.

On the other hand, in saline soils, the ionic strength (I) of soil solutions and the concentrations of ligand anions are high[3]. The environmental implications of salinization in terms of uptake of metals by crops are yet to be fully assessed despite the importance of metal uptake by crops[4]. It has been postulated that under saline conditions, high chloride (Cl^-) concentrations in soil solution could increase the degree to which metals like Cu, Cd, etc. are chloro-complexed[5]. Chloro-complexation raises total metal concentration in solution[6] and could lead to enhanced metal uptake by crops through either faster metal diffusion to roots or greater metal uptake if chloro-complexes are transported across the root membrane[4]. On these accounts chemical speciation of trace metals in aquatic media is considered as an important area of research and electrochemical methods are best applied in speciation studies.

1.2 Principle of Cyclic Voltammetry

Cyclic voltammetry (CV) is a class of potentiodynamic electrochemical measurement. It is one of the most commonly used electrochemical techniques for acquiring qualitative information about the electrochemical reactions. It is based on a linear potential waveform (**Fig. 1.1**); that is, the potential is changed as a linear function of time. The rate of change of potential with time is referred to as the *scan rate*. The triangular waveform produces the forward and the reverse scan. The potentials at which reversal takes place are called switching potentials.

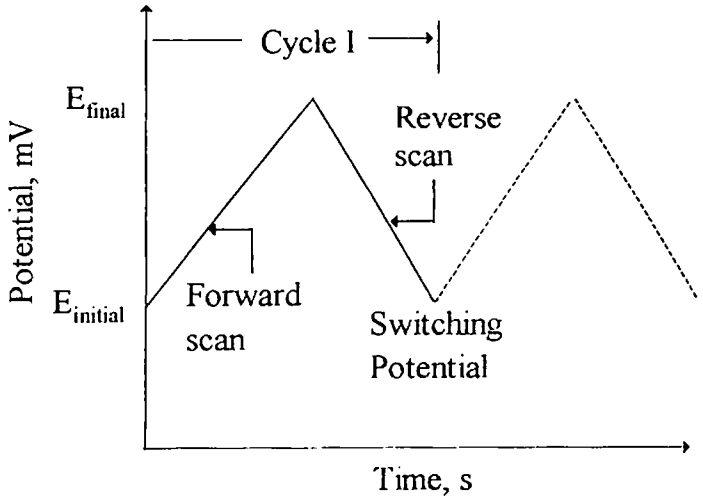

Fig. 1.1. Potential-time excitation signal in cyclic voltammetric experiment.

In a cyclic voltammetry experiment, a potential is applied to the system, and the faradaic current response is measured. The current response over a range of potentials is measured, starting at an initial value and varying the potential in a linear manner up to a pre-defined limiting value. At this potential, the direction of the potential scan is reversed, and the same potential window is scanned in the opposite direction (hence the term cyclic). This means that species formed by oxidation on the first scan can be reduced on the second scan. For a given experiment, switching potentials are chosen so that we can observe a diffusion-controlled oxidation or reduction of one or more species. The direction of the initial scan may be either negative, or positive, depending on the composition of the sample.

This technique is commonly used, since it provides a fast and simple method for initial characterization of a redox-active system. In addition to providing an estimate of the redox potential, it can also provide information about the rate of electron transfer between the electrode and the analyte, and the stability of the analyte in the electrolyzed oxidation states. **Fig. 1.2** illustrates a typical cyclic voltammogram.

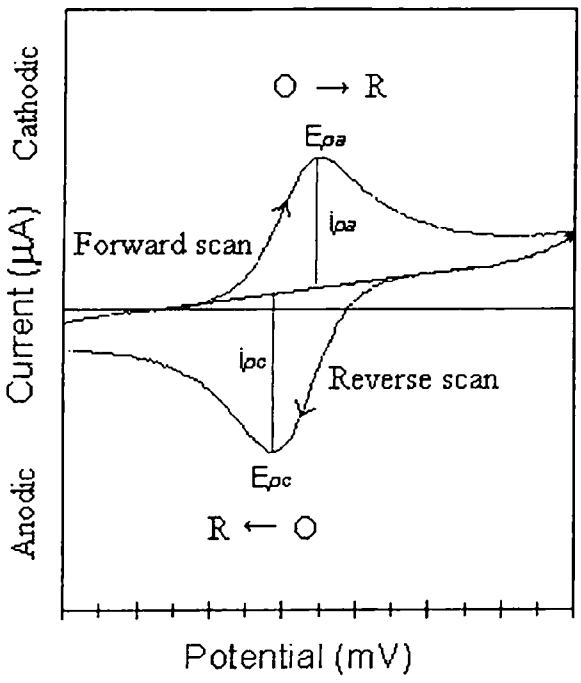

Fig. 1.2 A typical cyclic voltammogram showing the important parameters.

It is assumed that only the oxidized form O is present initially. Thus, a negative-going potential scan is chosen for the first half-cycle, starting from a value where no reduction

occurs. As the applied potential approaches the characteristic E^0 for the redox process, a cathodic current begins to increase, until a peak is reached. After traversing the potential region in which the reduction process takes place, the direction of the potential sweep is reversed. During the reverse scan, R molecules are reoxidized back to O and an anodic peak results.

There are three modes of mass transport that influence the rate at which reactants and products are transported to and from the electrode surface:

(i) Diffusion – the spontaneous movement under the influence of concentration gradient, aimed at minimizing concentration differences.

(ii) Migration – movement of charged particles along an electrical field.

(iii) Convection – transport to the electrode by a gross physical movement; such flow of the solution occurs with stirring or with rotation or vibration of the electrode.

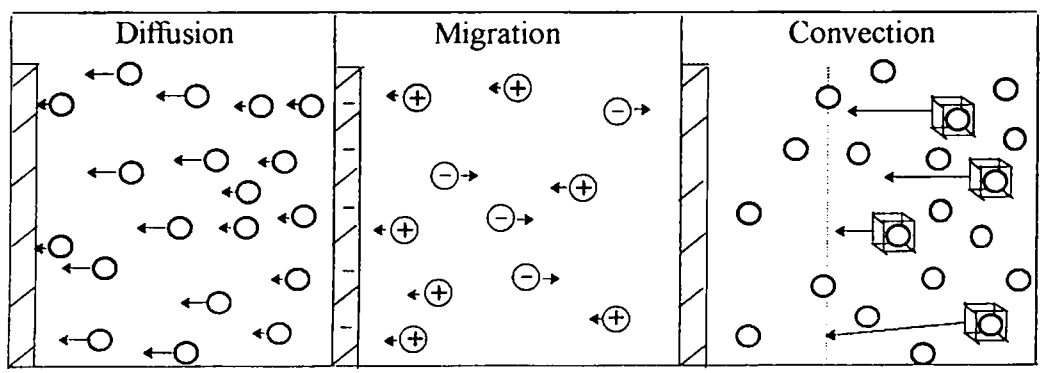

Fig. 1.3 The three modes of mass transport.

Suppression of the electromigration and convection can be achieved by the addition of excess inert electrolyte, also called a supporting electrolyte and use of a quiescent solution respectively. Under this condition, the movement of the electroactive species is limited by diffusion. In the limit in which diffusion is the only significant means for the mass transport of the reactants and products, the current in a voltammetric cell is given by

$$i = nFAD(C_{bulk} - C_{x=0})/\delta$$

where, n is the number of electrons transferred in the redox reaction, F is Faraday's constant, A is the area of the electrode, D is the diffusion coefficient for the reactant or

product, C_{bulk} and $C_{x=0}$ are the concentration of the analyte in bulk solution and at the electrode surface, and δ is the thickness (typically of 0.001 – 0.01 cm) of the diffusion layer.

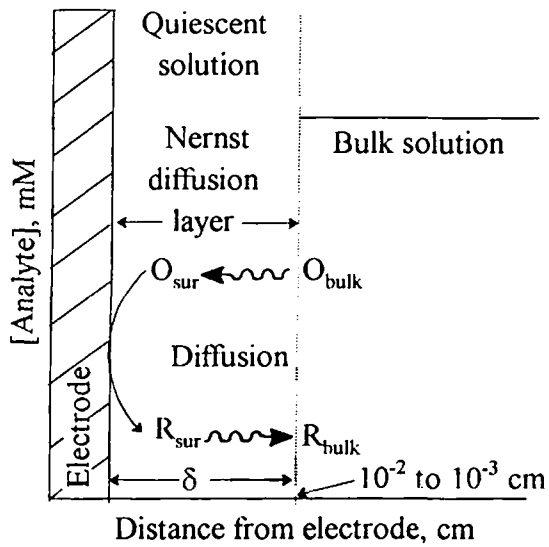

Fig. 1.4 Concentration gradient for the analyte showing the effects of diffusion as methods of mass transport

Thus the characteristic peaks in the cyclic voltammogram are caused by the formation of the diffusion layer near the electrode surface. According to Nicholson and Shain[7], the important parameters in a cyclic voltammogram are the cathodic peak potential E_{pc}, the anodic peak potential E_{pa}, the cathodic peak current i_{pc}, and the anodic peak current i_{pa}. The definitions and measurements of these parameters are illustrated in Fig. 1.2.

If a redox system remains in equilibrium throughout the potential scan, the electrochemical reaction is said to be reversible. In other words, equilibrium requires that the surface concentrations of O and R be maintained at the values required by the Nernst equation. Under these conditions, the following parameters characterize the cyclic voltammogram of the redox process.

(i) the peak potential separation (E_{pa} - E_{pc}) is equal to 59/n mV (in practice, the difference is typically 60/n – 70/n mV) for all scan rates at 25 ^{0}C where n is the number of electron equivalents transferred during the redox process.

(ii) the peak width is equal to 28.5/n mV for all scan rates.

(iii) the peak current ratio (i_{pa}/i_{pc}) is equal to 1 for all scan rates.

(iv) the peak current function ($ip_c/v^{1/2}$) increases linearly as a function of the square root of scan rate, v. A plot of the log I_p versus log v is linear, with a slope of 0.5 for a diffusion peak and a slope of 1 for an adsorption peak.

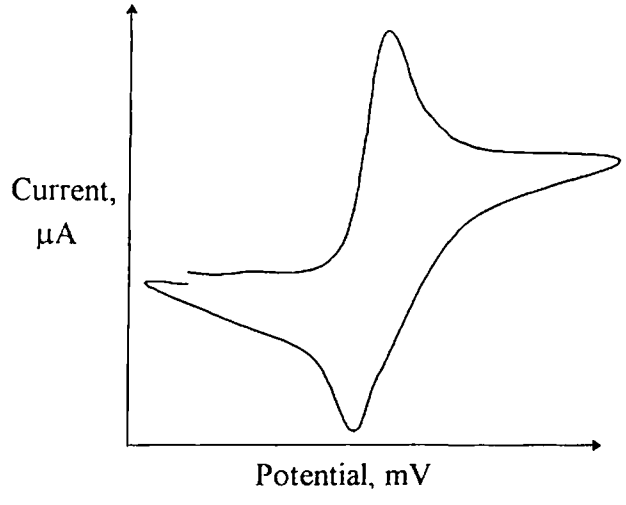

Fig. 1.5 Cyclic voltammogram for a reversible O + e⁻ ⇌ R redox process.

For a reversible electrode reaction, anodic and cathodic peak currents are approximately equal in absolute value but opposite in sign (**Fig. 1.5**). The peak current for a reversible couple is described by the Randles-Sevcik equation[8]:

$$i_p = (2.686 \times 10^5)\, n^{3/2} A C D^{1/2} v^{1/2} \qquad (1)$$

where n is the number of electrons, A is the electrode area in cm^2, C is the concentration in mol cm^{-3}, D is the diffusion coefficient in $cm^2\ s^{-1}$, and v is the scan rate in $V\ s^{-1}$. Accordingly, the current is directly proportional to concentration and increases with the square root of the scan rate.

The position of the peaks on the potential axis (E_p) is related to the formal potential of the redox process. The formal potential for a reversible couple is centered between E_{pa} and E_{pc}:

$$E_{1/2} = \frac{E_{pa} - E_{pc}}{2} \qquad (2)$$

For multielectron-transfer (reversible) process, the cyclic voltammogram consists of several distinct peaks if the $E_{1/2}$ values for the individual steps are successively higher and are well separated (**Fig. 1.6**).

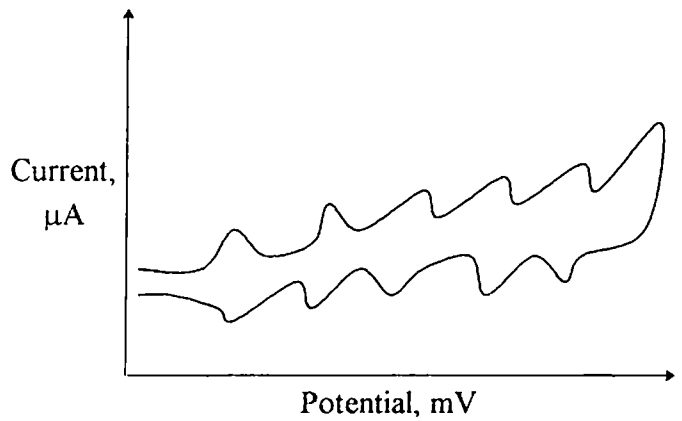

Fig. 1.6 Cyclic voltammogram of a reversible multi-electron transfer process.

Departures from reversible behavior for a redox process arise due to two main causes:

(i) Slow Electron Transfer Kinetics: Reversibility requirs that the electron transfer kinetics are fast enough to maintain the surface concentrations of O and R at the values required by the Nernst equation. Hence, reversibility depends on the relative values of the standard heterogeneous electron transfer rate constant (k^0) and the rate of change of potential - the scan rate, ν. If the ratio of k^0/ν is sufficiently small that Nernstian concentrations cannot be maintained, then the process is said to be *quasi-reversible*.

(ii) *Chemical Reactions of O and R:* Equilibrium values of O and R can only be maintained during a cyclic voltammetry experiment if both O and R are stable on the experimental time scale. For example, if the reduction of O to R is followed by the conversion of R to P, then more R must be generated to compensate for the loss of R. Therefore, the rate of reduction increases and E_{pc} moves to a more positive value. In addition, i_{pa}/i_{pc} is less than unity since only a fraction of the molecules that were reduced on the forward scan are available for reoxidation on the reverse scan. The value of the current function can also be affected by chemical reactions following electron transfer.

For irreversible processes (those with sluggish electron exchange), the individual peaks are reduced in size and widely separated (**Fig. 1.7**).

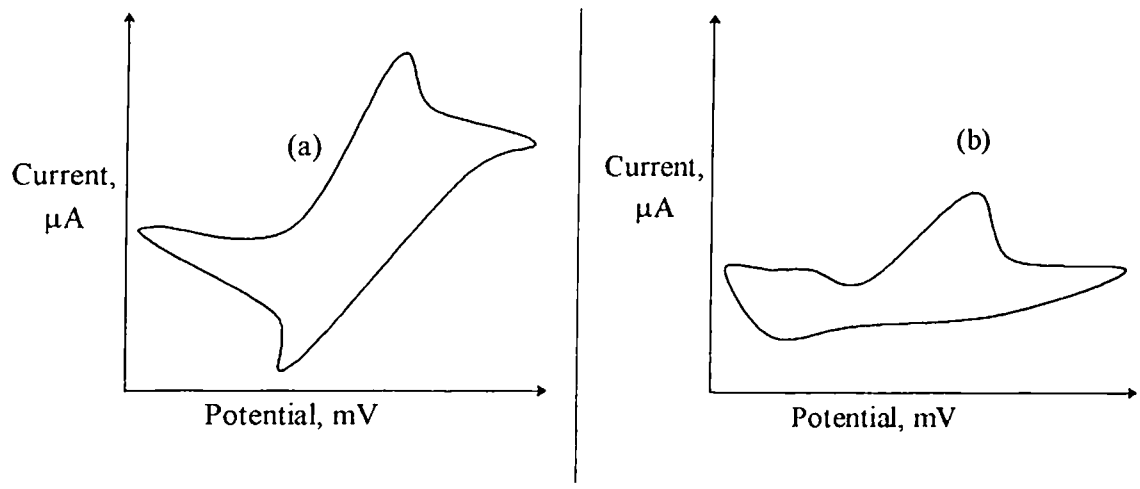

Fig. 1.7. Cyclic voltammograms for (a) quasi-reversible and (b) irreversible electrode reactions.

Totally irreversible systems are characterized by a shift of the peak potential with the scan rate:

$$E_p = E^0 - \frac{RT}{\alpha n_a F}\left(0.78 - \ln\frac{k^o}{D^{1/2}} + \ln\left(\frac{\alpha n_a F \nu}{RT}\right)\right)^{1/2} \qquad (3)$$

Where α is the transfer coefficient and n_a is the number of electrons involved in the charge-transfer step. Thus E_p occurs at potentials higher than E^0, with the over-potential related to k^0 and α. Independent of the value of k^0, such peak displacement can be compensated by an appropriate change of the scan rate. The peak potential and the half-peak potential at 25 ^{0}C will differ by $48/\alpha n$ mV. Hence the voltammogram becomes more drawn-out as αn decreases.

The peak current is given by

$$I_p = (2.99 \times 10^5) n(\alpha n_a)^{1/2} A C D^{1/2} \nu^{1/2} \qquad (4)$$

is still proportional to the bulk concentration, but will be lower in height (depending upon the value of α).

Qualitatively, the demarcation point separating quasi-reversible from irreversible has been reached when there is no (potential) overlap between the cathodic and anodic peak shapes. For quasi-reversible systems with $10^{-1} > k^0 > 10^{-5}$ cm s^{-1}, the current is controlled by both the charge transfer and mass transport. The shape of the cyclic voltammogram is

a function of $k^0/\sqrt{(\pi aD)}$ (where $a = nF\nu/RT$). As $k^0/\sqrt{(\pi aD)}$ increases, the process approaches the reversible case. For small values of $k^0/\sqrt{(\pi aD)}$ (i.e., at very fast ν) the system exhibits an irreversible behavior. Overall the voltammograms of a quasi-reversible system are more drawn-out and exhibit a larger separation in peak potentials compared to those of a reversible system (**Fig. 1.5**).

The basic instrumentation required for voltammetric measurements include a cell, a software driven voltammetric analyzer and a recorder. Modern voltammetric analyzers are versatile enough to perform many modes of operation. The material for cell construction is Pyrex glass for reasons both of visibility and general chemical inertness. The size of the cell is variable and depends upon the volume, cost and degree of dilution of the sample being studied. The cell used for voltammetric measurements is made up of three electrodes (**Fig. 1.8**) immersed in a solution containing the analyte and also an excess of a nonreactive electrolyte called a supporting electrolyte. The cell lid is made from resistant PTFE plastic. One of the three electrodes is the working electrode, whose potential is varied linearly with time. This is the electrode at which the electrochemical phenomena being investigated takes place. The second electrode is the reference electrode. This is the electrode whose potential is constant enough that it can be taken as the reference standard against which the potentials of the other electrodes present in the cell can be measured. The third electrode is the auxiliary or counter electrode that simply serves to conduct electricity from the signal source through the solution to the working electrode.

The reference electrode is placed as close as possible to the working electrode and is connected to the instrument through a high-resistance circuit that draws no current from it. Hence the current flows through the solution between the working and the auxiliary electrodes only. Symmetry in the placement of these electrodes is important for the assumption that the current paths from all points on the working electrode are equivalent. Because no current passes through the reference electrode and because of its position close to the working electrode, the ohmic potential drop caused by the cell resistance (iR) is minimized.

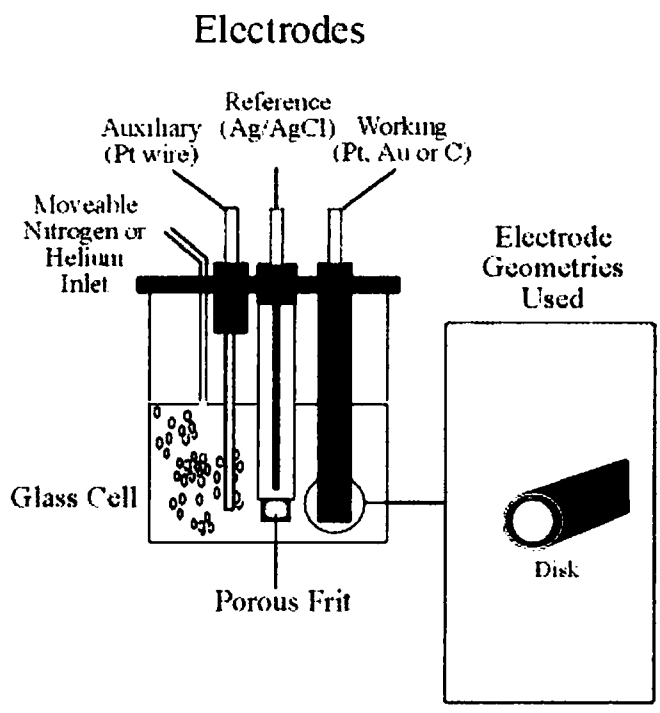

Fig. 1.8 A typical voltammetric cell.

Solid disk microelectrodes are most commonly employed in cyclic voltammetry experiments. The electrodes can be stationary or rotating, usually in a planar disk configuration. Such electrodes consist of a short cylindrical rod of the electrode material embedded in a tightly fitting tube of an insulating material (Teflon, Kel-F *etc.*). It is essential to avoid crevices between the sleeve and the electrode materials, and thus to prevent solution creeping and thus an increased background response. Electrical contact is made at the rear face.

The material of the working electrode plays a very vital role in performance of the voltammetric procedure. Its selection depends primarily on two factors: the redox behavior of the target analyte and the background current over the potential region required for the measurement. Other considerations include the potential window, electrical conductivity, surface reproducibility, mechanical properties, cost, availability, and toxicity. Some very common voltammetry electrodes consist of glassy carbon, platinum, and/or gold. Glassy carbon has been very popular because of its excellent mechanical and electrical properties, wide potential window, chemical inertness (solvent resistance), and relatively reproducible performance. The material is prepared by means of a carefully controlled heating program of a premodeled polymeric resin body in an

inert atmosphere[9]. The structure of glassy carbon involves thin, tangled ribbons of cross-linked graphite-like sheets. Because of its high density and small pore size, no impregnating procedure is required. However, a surface pretreatment is usually employed to create active and reproducible glassy-carbon electrodes and to enhance their analytical performance[10,11]. Such pretreatment is usually achieved by polishing with successively smaller alumina particles on a polishing cloth. The electrode should then be rinsed with deionized water before use.

The ideal reference electrode should posses the following properties:

(i) it should be reversible and obey the Nernst equation with respect to some species in the electrolyte
(ii) its potential should be stable with time
(iii) its potential should return to the equilibrium potential after small currents are passed through the electrode
(iv) if it is an electrode like the Ag/AgCl reference electrode, the solid phase must not be appreciably soluble in the electrolyte, and
(v) it should show low hysteresis with temperature cycling.

The most common reference electrode systems used in aqueous solutions are Ag/AgCl and the calomel electrode.
An inert conducting material, such as platinum wire or graphite rod, is usually used as the current-carrying auxiliary electrode.

Oxygen is electrochemically active and its solubility in water is sufficiently great that oxygen reduction can be a problem. The electrochemical reduction of oxygen usually proceeds via two well-separated two-electron steps as shown in **Fig. 1.9**.

The half-wave potentials of these steps are approximately -0.1 and -0.9 V. The large background current acquiring from this stepwise oxygen reduction interferes with the measurement of many reducible analytes. In addition, the products of the oxygen reduction may affect the electrochemical process under investigation. As a consequence, most measurements are carried out under an inert atmosphere of either nitrogen or helium[12]. Thus a gas line for ebulliating the solution with nitrogen or helium is also evident.

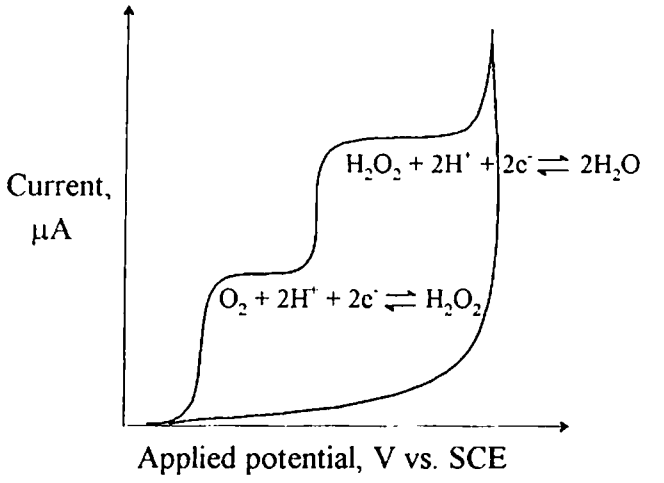

Fig.1.9 Voltammogram for the reduction of oxygen in an air-saturated 0.1 M KCl solution. The lower curve is for oxygen free 0.1 M KCl.

Cyclic voltammetric measurements are commonly carried out in a medium that consists of solvent containing a supporting electrolyte. The choice of solvent is determined primarily by the solubility of the analyte and its redox activity, and by solvent properties such as the electrical conductivity, electrochemical activity, and chemical reactivity[13]. While water has been used as a solvent more than any other media, nonaqueous solvents (*e.g.* acetonitrile, DMF, DMSO, or methanol) have also frequently been used.

The supporting electrolyte, added to enhance conductivity and to minimize double-layer and migration current effects[14], is chosen on the basis of solubility in a given solvent as well as inertness toward the electroactive substance and its electrolysis products. The inert supporting electrolyte may be an inorganic salt, a mineral acid, or a buffer. Potassium chloride or nitrate, ammonium chloride, sodium hydroxide, or hydrochloric acid is widely used when using water as a solvent, while tetraalkylammonium salts are often employed in organic media. Acetate, phosphate, or citrate buffer is used when a pH control is essential.

Although cyclic voltammetry is very widely used for the initial redox characterization of a molecule i.e., the redox potentials and the stability of the different oxidations states and for qualitative investigation of chemical reactions that accompany electron transfer, there are a number of disadvantages inherent in this technique:

(i) The effects of slow heterogeneous electron transfer and chemical reactions cannot be separated. If both of these effects are present, then the rate constants

for these processes can only be calculated using simulation methods.

(ii) There is a background charging current throughout the experiment of magnitude νC_{dl}, where C_{dl} is the capacitance of the interface at the working electrode. This restricts the detection limit to about 10^{-5} M. In addition, the ratio of the peak faradaic current to the charging current decreases with increasing ν since i_p is proportional to $\nu^{1/2}$, and this places an upper limit on the value of ν that can be used.

1.3 Theories of Chronocoulometry

Chronocoulometry (CC) is one of the classical electrochemical techniques frequently used in electroanalytical chemistry. As its name implies, CC is the measurement of the charge, (coulombs) as a function of time (seconds). The charge-time response of the potential step experiment is given by the Cottrell equation[15].

$$i = nFAC_O^b\left(\frac{Do}{\pi t}\right)^{1/2} \qquad (5)$$

For the limiting case of sufficiently negative E_{final}, this gives

$$Q = nFAC_O^b\left(\frac{D_O}{\pi t}\right)^{1/2} \qquad (6)$$

This technique is used for the measurement of the electrode surface area, diffusion co-efficient, concentration, kinetics of both heterogeneous charge transfer reaction and chemical reactions coupled to electron transfer adsorption and the effective time window of an electrochemical cell[16]. In this method, the current is integrated so that the monitored response is charge, Q[17-19]. Thus it involves measurement of charge *vs.* time response to an applied potential waveform. The shape of the resulting chronocoulogram is interpreted by considering the concentration gradients in the solution adjacent to the electrode surface. This technique yields information about the following parameter and phenomena[16-17].

(i) Electrode surface area,
(ii) Diffusion coefficient,
(iii) Concentration,
(iv) Kinetics and mechanism of coupled chemical reaction,
(v) Kinetics of heterogeneous electronics transfer,

(vi) Adsorption, and

(vii) The effective time window of an electrochemical cell.

Double potential step chronocoulometry is performed by applying a potential step to the working electrode[19-21]. The potential is stepped from an initial value to a second value and then back to the initial value. The step from initial to the second is termed as forward potential step, whereas the step from the second to the initial value is termed as reverse step[21]. A good understanding in chronocoulometry requires consideration of the solution and interfacial phenomena that accompany the potential step excitation signal[21].

The effects of the changes in potential used in the chronocoulometric experiment can be understood by considering the Nernst equation, which relates the applied potential E, (in V), the formal redox potential $E^{o'}$ and the surface concentrations (C^S) of the electroactive species[22].

For the redox couple

$$O + ne^- \rightleftharpoons R \qquad (7)$$

at 25 °C can be given by

$$E = E^{o} - 2.303\frac{RT}{nF}\log\left(\frac{C_{R(0,t)}}{C_{O(0,t)}}\right) \qquad (8)$$

It is apparent from equation (8) that changes in the excitation signal causes changes in the ratio of surface concentration C^S_R / C^S_O.

The change is simply accomplished by the reduction or oxidation of 'O' or 'R' respectively as in equation (8) and the resulting electrolysis causes current.

1.3.1 Charge-Response Signal

The charge response signal for a double potential step chronocoulometry is charge due to electrolysis of 'O' or 'R' as in equation (7). It involves application of a forward potential step, causing reduction of 'O' at the condition $C_{R(0,t)} = 0$ followed at time τ by reverse potential step causing reoxidation of the product R (generated during $t < \tau$) at the condition $C_{R(0,t)} = 0$. Consider applying to a working electrode a potential step sufficiently negative that the concentration of the reactant species O is forced immediately to an essentially zero value.

$$C_{O(0,t)} = 0 \qquad (9)$$

For an experiment controlled by O diffusion, the used initial condition is that of a homogeneous solution at t = 0,

$$C_{O(x,0)} = C_o^b \qquad (10)$$

The boundary condition semi-infinite diffusion is

$$C_{O(\infty,t)} = C_o^{bulk} \qquad (11)$$

Applying equation (9) and boundary conditions (10) and (11) to Fick's law for O, yields an expression for the concentration of O as a function of time and distance from the electrode surface is obtained as

$$C_{O(x,t)} = C_O^b \mathrm{erf}\left[\frac{x}{2D_O^{1/2}t^{1/2}}\right] \qquad (12)$$

where erf denotes error function. Diffusion layer thickness is crudely approximated by the term $(D_0t)^{1/2}$cm. The current flow is proportional through Fick's First Law, to the instantaneous concentration gradient of O at the electrode surface. Accordingly,

$$i = nFD_O\left(\frac{\partial C_{O(0,t)}}{\partial x}\right) \qquad (13)$$

which, when applied to the differentiated equation (12) gives the *Cottrell* equation

$$i = nFAC_O^b\left(\frac{D_O}{\pi t}\right)^{1/2} \qquad (14)$$

The Cottrell equation shows that diffusion controlled electrolysis of reactant 'O' at a planar, stationary electrode gives a current as a $t^{-1/2}$ function which is proportional at any given time to the bulk concentration of electrode reactant. A current vs. $t^{-1/2}$ plot is called a Cottrell plot and its linearity (with zero intercept) constitutes a criterion for simple diffusion control of the electrolysis rate. For reversible charge transfer, simultaneous solution of Fick's law for 'O' and 'R' and use of equation (8) and other appropriate boundary conditions[23] give

$$i = nFC_o^b\left(\frac{D_{Ox}}{\pi t}\right)^{1/2}\left\{1+\left(\frac{D_O}{D_R}\right)^{1/2}\exp\left[\frac{nF}{RT}\left(E-E^0\right)\right]\right\}^{-1} \qquad (15)$$

The chronocoulometric or response of the potential step experiment is elicited from (13) and (15) simply by integrating the current-time equation. For the case of sufficiently negative E_{final}, this gives

$$Q = 2nFC_O^b\left(\frac{D_O t}{\pi}\right)^{1/2} \qquad (16)$$

At times $t < \tau$ the current and charge time curves are described by (12) and (16).

Equation (16) shows that the diffusion component to the charge is zero at t = 0, yet a plot of the total charge, Q vs. $t^{1/2}$ generally does not pass though the origin, because additional components arise from the double layer charging and from the electro reduction of any O molecules that be adsorbed at Ei.

At times $t > \tau$ the oxidation of 'R' occurs from the diffusion layer of 'R' created during the negative potential step. The diffusion profile of 'R' at time τ is thus in effect the initial condition of reverse potential step. The 'R' diffusion profile is connected to that of 'O' by the expression stating that the flux of 'R' leaving the electrode surface equals that of 'O' arriving

$$D_O \frac{\partial C_{O(0,t)}}{\partial x} = -D_R \frac{\partial C_{R(0,t)}}{\partial x} \qquad (17)$$

Applying these conditions to a Fick's law solution one can obtain the diffusion profile of 'Red' for $t<\tau$

$$C_{R(x,t)} = C_O^b\left(\frac{D_O}{D_R}\right)^{1/2} \text{erfc}\left[\frac{x}{2D_O^{1/2}t^{1/2}}\right] \qquad (18)$$

Where erfc is the complementary error function.

On the basis of equation (18) Christie[23] obtained an expression (19) for i_a when $t > \tau$ for reverse potential step. Consequently,

$$i_a = \frac{nFD_O^{1/2}C_O^b}{\pi^{1/2}}\left[\frac{1}{(t-\tau)^{1/2}} - \frac{1}{t^{1/2}}\right] \qquad (19)$$

Consequently,

$$Q_a = \frac{2nFD_O^{1/2}C_O^b}{\pi^{1/2}}\left[t^{1/2} - (t-\tau)^{1/2}\right] \qquad (20)$$

where i_a and Q_a represent the anodic current and charges respectively at time $t > \tau$.

Consider the case in which at t = 0, 'O' is in equilibrium between its adsorbed and solution forms:

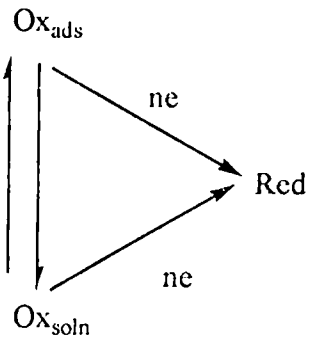

Both O_{ads} and O_{soln} are presumed to be electroactive. Application of a potential step sufficiently negative to produce $C_{O(soln)(o,\,t)} = C_{O\,(ads)(o,\,t)} = 0$ yield the normal diffusional current- time response for electrolysis of O_{soln}, but the adsorbed species O_{ads} does not require mass transport step prior to reduction and present in a limited amount determined by the surface excess of O_{ads} (Γ_0 at t = 0). To record chronocoulometric (Q-t) response the charge attributable of the O_{ads} is considered to be

$$Q_{ads} = nF\Gamma_0 \qquad (21)$$

The expression for the chronocoulometric response in the presence of reactant adsorption is then

$$Q = 2nFC_O^b\left(\frac{D_O t}{\pi}\right)^{1/2} + Q_{ads} + Q_{dl} \qquad (22)$$

where, C^b_{ox} is the bulk concentration of O_{soln} and Q_{dl} is the difference in the charge on the electrical double layer between $E_{initial}$ and E_{final} of the potential step and Q_{ads} represent $nF\Gamma_0$ at E_{init}. The zero time intercept of a plot of Q - $t^{1/2}$ provides $Q_{ads} = Q_{dl}$. After correction for Q_{dl} the surface excess Γ_0 can be obtained from equation (22).

The correction for Q_{dl} is obtained from a potential step from E_{init} to E_{final} in supporting electrolyte solution alone. The chronocoulometric method of adsorption measurement was used by Christie and co-workers[24].

$$Q = 2nFC_O^b\left(\frac{D_O t}{\pi}\right)^{1/2} + nFA\Gamma_0 + Q_{dl} \qquad (23)$$

Double potential step experiment, introduced by Anson[25] and theoretically characterized by Christie and associates[26], eliminates much of the experimental error incurred in the Q_{dl} correction by acquiring $Q_{dl} + Q_{ads}$ and Q_{dl} data in a single experiment. In a double potential step chronocoulometric experiment with reactant adsorption at $t \leq \tau$ is given by equation (22) and at $t > \tau$[26] is given by equation (23)

$$Q_a = 2nFC_O^b\left(\frac{D_O t}{\pi}\right)^{1/2} \times \left[\tau^{1/2} + (t-\tau)^{1/2}\right] + Q_{ads}\left(\frac{2}{\pi}\sin^{-1}\left(\frac{\tau}{t}\right)^{1/2}\right) \quad (24)$$

This expression describing charge for oxidation of 'R', differs from the diffusion only equation (20) only by the last term, which accounts for the extra quantity of 'R' arising from previous reduction of O_{ads}. This term is small and well approximated by a simple expression; making such an approximation and now measuring charge as a difference between Q_a and the cathodic charge at τ gives

$$Q_r - Q_a = 2nFC_O^b\left(\frac{D_O}{\pi}\right)^{1/2}\left[1 + \frac{a_1\Gamma_0\pi^{1/2}}{2C_O^b D_O^{1/2}\tau^{1/2}}\right] \times \left[\tau^{1/2} + (t-\tau)^{1/2} - t^{1/2}\right] + a_0 Q_{ads} + Q_{dl} \quad (25)$$

The term a_0 and a_1 are constants and typical values[27] are $a_0 = -0.0688$ and $a_1 = 0.970$.

Experimental data are treated according to (23) and (25) by plots of Q_c vs $t^{1/2}$ and $Q_r - Q_a$ vs. $[(t-\tau)^{1/2} + \tau^{1/2} - t^{1/2}]$. Comparison to (23) and (25) shows the intercept of these plots are $Q_{ads} + Q_{dl}$ and $a_0Q_{ads} + Q_{dl}$: the difference between these intercepts eliminates Q_{dl} and is $Q_{ads}(1-a_0)$ allowing calculation of Γ.

This theory assumes, in expressing the Q_{dl} for E_{init} at $t > \tau$, instantaneous reestablishment of the O_{ads} layer after the reverse potential step.

A plot of Q $(t > \tau)$ vs. $t^{1/2} - (t-\tau)^{1/2}$ must pass through origin if neither reactant "O" nor product "R" in equation (7) are specifically adsorbed on the electrode surface. If we consider the following equation derived by Kambara[28-29]:

$$Q_r = 2nFC_O^b\left(\frac{D_O t}{\pi}\right)^{1/2} \times \left[\tau^{1/2} + (t-\tau)^{1/2} - t^{1/2}\right] + Q_{dl} \quad (26)$$

where, $Q_r = Q_\tau - Q(t>\tau)$ (27)

and, $Q_r = 2nFC_O^b\left(\frac{D_O t}{\pi}\right)^{1/2} + Q_{dl}$ (28)

Now if Q value obtained from time less than τ is plotted versus $t^{1/2}$ and on the same graph $-Q_r$ is plotted versus $[\tau^{1/2} - (t-\tau)^{1/2} - t^{1/2}] = \Theta$, there will be two straight lines which intersects each other at $Q = 0$ axis with equal slope, if there is no adsorption of reactant or product[30]. Any deviation from such condition means adsorption.

The charge response signal for double potential step chronocoulometry is charge due to the electrolysis of 'O' or 'R' as in equation (7). The concentration profile of Co(x, t) can be given by the following equation[31],

$$\frac{\partial C_{o(x,t)}}{\partial t} = D_o \frac{\partial^2 C_{o(x,t)}}{\partial x^2} \quad (29)$$

where, Co = concentration of 'O' (mol cm^{-1})

Do = Diffusion co-efficient of 'O' (cm^2 s^{-1})

t = time in second and x is between zero to infinity

Now solving equation (29) with Laplacian transformations[32]. We get

$$\text{flux}[= J_o(0,t)] = \frac{i}{nFA} = D_o \frac{\partial C_{o(x,t)}}{\partial x} \quad (30)$$

$$i_t = \frac{nFAD_o^{1/2}C_o}{t^{1/2}} \quad (31)$$

where, it = current (amp) at time t.

n = no. of electrons transferred per ion or molecule (eq. mol^{-1}).

F = Faraday's constant (approximately 96500 coulomb)

A = area of the electrode (cm^2).

The inversion of equation (31) produces the current time response. The equation is known as Cottrell equation and can be represented by the following way,

$$i = \frac{nFAD_o^{1/2}C_o}{\pi^{1/2}t^{1/2}} \quad (32)$$

The equation that describes the result in charge (Q) versus time (t) curve for the forward step is the integral of equation (32) and can be given by the following equation,

$$Q = \frac{2nFC_oD_o^{1/2}t^{1/2}}{\pi^{1/2}} = 2Kt^{1/2} \quad (33)$$

According to this equation Q increases as a function of $t^{1/2}$ during the forward potential step giving the total amount of 'O' that is reduced and 'R', which produces. This Q is a measure of the amount of material electrolyzed up to that time[33]. The reverse potential step at time 'τ' initiates an anodic electrode reaction.

From equation (23) a plot of Q vs $t^{1/2}$ gives a straight line of

$$\text{slope} = \frac{2nFAC_O^0D^{1/2}}{\pi^{1/2}} \quad (34)$$

$$\text{and intercept} = Q_{dl} + nFA\Gamma_0 \quad (35)$$

The electrode area is obtained from equation (34) is

$$A = \frac{\text{slope} \times \pi^{1/2}}{2nFC_O^0 D^{1/2}} \qquad (36)$$

Thus using an electroactive species of known diffusion co-efficient and concentration, the value of electrode can be evaluated and the charge transfer rate constant can be deduced[34].

$$\text{So, } k_f = \frac{\text{slope} \times H \times \pi^{1/2}}{2nFAC_O^0} \qquad (37)$$

$$\text{where, } H = \frac{\pi^{1/2}}{2t_i^{1/2}} \qquad (38)$$

$t_i^{1/2}$ can be obtained by extrapolating the straight line obtained from the plot of background charge *vs.* $t^{1/2}$.

1.4 Composition of a Complex

Molecular absorption, particularly in the UV/VIS range, has been used for a variety of different characterization studies, including determining the stoichiometry of metal-ligand complexes and determining equilibrium constants. The stoichiometry for a metal-ligand complexation reaction of the following general form :

$M + nL \rightarrow ML_n$ (where, M is a metal ion and L may be a ligand, mono-, bi- or multidentate) can be determined by one of three methods: the method of continuous variation, the mole-ratio method, and the slope-ratio method. Of the three methods, the method of continuous variation, also called Job's method, is a simple and effective approach to the determination of reaction stoichiometry. This method was first employed by Job and later modified by Vosbourgh and Copper[35].

A series of solutions is prepared in which the sum of the number of moles of M and the number of moles of L is kept constant, but in which the relative amounts of M and L are systematically varied. The challenging aspect of the application of Job's method is in finding a way to measure the amount of product formed in each solution. If the product absorbs light at a known wavelength, then each solution can be placed in a spectrometer and the absorbance at that wavelength determined. If the product precipitates, the product in each solution may be recovered by filtration and weighed. There are many other possibilities.

Spectrophotometric method is the most common one. One great advantage of this method is that the quantitative measurements can be made without affecting the equilibrium being studied. In most of the systems involving complex formation either any reactant or product, absorbs but it is not necessary, and in fact any component after taking part in the competitive equilibria may produce absorbing species.

The absorbance of each solution is measured at the λ_{max}. The difference between the measured absorbance and the absorbance calculated for the mixed constituents on the assumption of no reaction between them is plotted against the mole fraction of one of the constituents. The mole fraction of the ligand can be represented as $X_L/ (X_M + X_L)$, where X_L and X_M are the mole fractions of ligand and metal respectively. Fig. 1.9 shows a maximum at a certain X_L/ X_M ratio, which corresponds to the ratio of metal to ligand in the complex.

Normally the plot looks like an inverted "V", with the vertex skewed toward one side or the other. If the formation constant of the complex is small, a significant curvature results. Then straight lines are drawn through the points on both sides of the vertex, and the mole of L corresponding to their intersection point allows the stoichiometry to be determined. The value of n is then calculated using the following equation:

n = (moles of L at intersection)/[total moles M + L – moles of L at intersection]

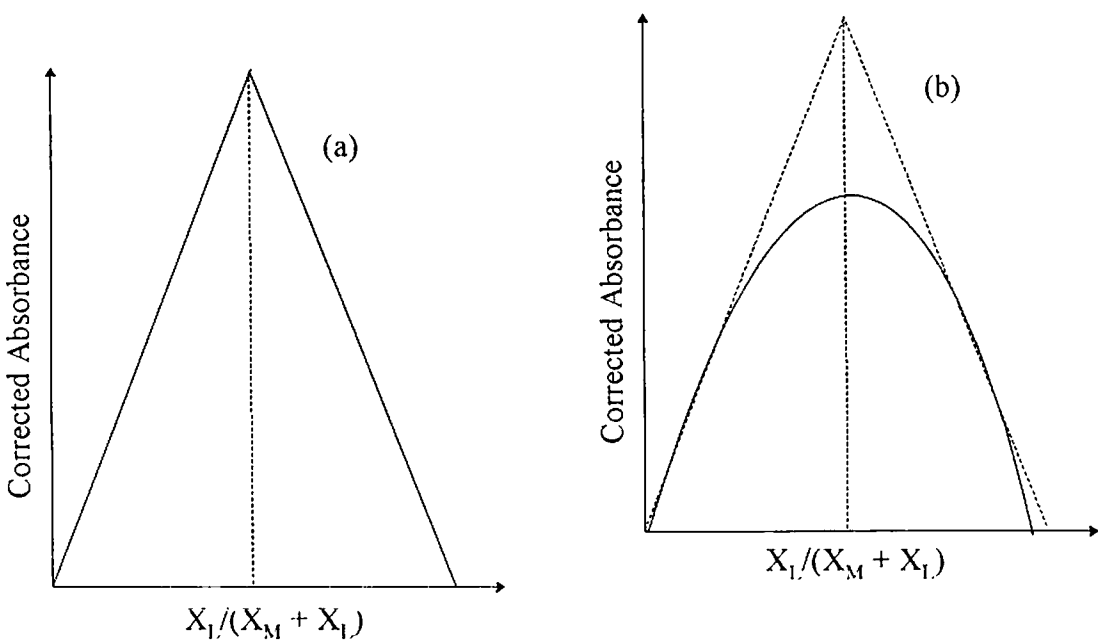

Fig. 1.9 Continuous variation curve for complex, ML_n, having a (a) large and (b) small formation constant.

The discussion on the methods used commonly in the visible region is also equally applicable in the ultraviolet methods. The primary difference between these two methods is that ions, molecules or atoms absorbing in the ultraviolet region absorb more energy for excitation than in the visible region. In many substances, which are colorless for the visible region electronic excitations do occur because of the absorption of ultraviolet radiation.

1.5 Catechol as a Complexing Ligand

Pyrocatechol[36], more commonly known as catechol, is a benzenediol, with the formula $C_6H_4(OH)_2$. It was first isolated in 1839 by H. Reinsch by distilling catechin (the juice of *Mimosa catechu* (*Acacia catechu* L.f)); it occurs free in kino and in beechwood tar; its sulfonic acid is present in the urine of horse and man.

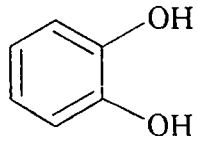

Catechol

Some of the physical properties of catechol are given below:

Synonyms	Pyrocatechol, Catechol, Benzene-1,2-diol, *o*-Benzenediol, 1,2-dihydroxybenzene, 2-hydroxyphenol, α-hydroxyphenol, *o*-hydroxyphenol, pyrocatechin
Formula	$C_6H_6O_2$
Molecular weight	110.1
Physical state	white solid, faint phenolic odor
Melting point	105 ^{0}C
Boiling point	245.5 ^{0}C
Specific gravity	1.344
Solubility in water	43 g/100 mL
Stability	Stable under ordinary conditions (light sensitive)

Small amounts of catechol occur naturally in fruits and vegetables, along with the enzyme polyphenol oxidase. Upon exposure to air (as when a potato or apple is cut), the colorless catechol oxidizes to reddish-brown benzoquinone. This accounts for the browning of cut fruit and vegetables[37].

Catechol is used as a photographic developer, a developer for fur dyes, as an intermediate for antioxidants in rubber and lubricating oils, in polymerization inhibitors, and in pharmaceuticals.

Catechol is the conjugate base of a chelating agent used widely in coordination chemistry. Basic solutions of catechol react with iron(III) to give the red $[Fe(C_6H_4O_2)_3]^{3-}$. Ferric chloride gives a green coloration with the aqueous solution, whilst the alkaline solution rapidly changes to a green and finally to a black color on exposure to the air. It reduces silver solutions in the cold and alkaline copper on heating. Catechol can also be conjugated to ruthenium. $[Ru^{III}(NH_3)_4(catechol)]^{+}$ oxidizes faster than catechol in the presence of oxygen, but controlled potential electrolysis showed that its oxidation involves only one electron[38].

Catechol molecule has two hydroxyl groups; the hydrogens of which are fairly strongly acidic. Removal of one or both hydrogens from a catechol molecule would produce a catechol anion having a negative center on the oxygen atom(s); the anion could then co-ordinate with a suitable metal atom or ion.

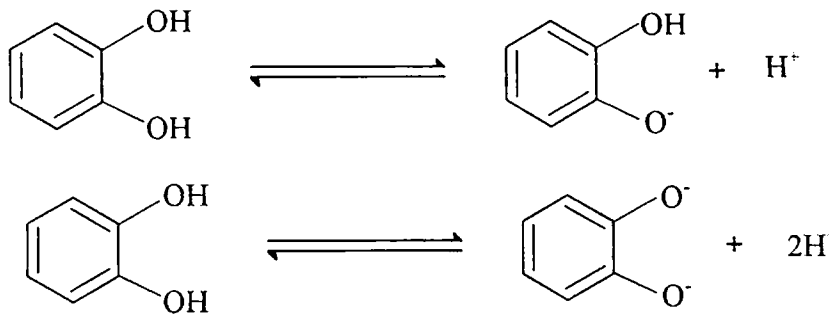

The negative charge on oxygen(s) may undergo delocalization over the ring to some extent, which also enable catechol anion to interact with metal ions under suitable conditions. Thus catechol anion can form both ionic and molecular complexes with different metal ions in different ways. The following modes of linkages of catechol anion with metal ions are possible:

(i) The catechol anion can act as a monodentate ligand by forming bond through oxygen.

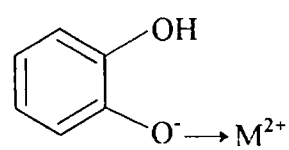

(ii) It can behave as bidentate ligand both in the bridging and chelating modes.

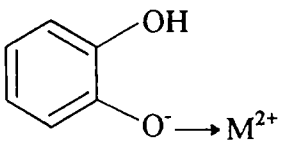

Bridiging

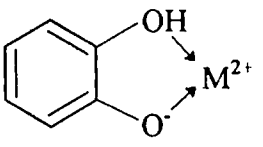

Chelating

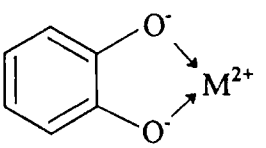

Chelating

(iii) There could be π-interaction involving the phenyl ring.

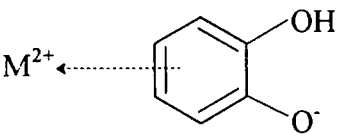

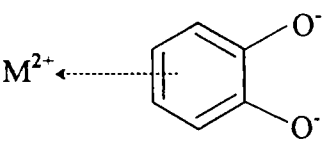

(iv) On the surface of electrode where removal of electrons is possible the catechol dianion can be converted to quinone that can behave like a bidentate ligand.

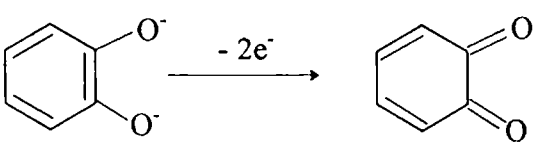

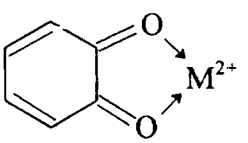

1.6 A Brief Review of Previous Work Related to This Study

The concept of the chemical speciation of trace metals and their biological activity is very recent. The crucial importance of defining the speciation (physicochemical forms) of metal in water is now well established[39-41]. However, our knowledge of metal speciation is still inadequate and the available results are often confusing and contradictory[42].

Organic compounds like glycine, cysteine catechol, humic acid etc. reduces heavy metals toxicity to aquatic lives by complexing free ions which are primarily responsible for biotoxicity[40].

The degree of complexation, complexation parameters and the complexes so formed may be estimated in a number of ways, e.g. voltammetric, ion-selective, and ion exchange method followed by AAS, etc. Recently, a comprehensive study on metal speciation in

water and its importance to biota has been reviewed by several authors[43-47].

Studies of organic complexation of trace metals in natural waters have revealed consistently that a large proportion of several trace metals occur in the complex form with dissolved organic matters. But the fraction of metal observed complexed through experiments differs from the theoretical values[48]. It is to be expected that difference in complexation occurs between metals and samples from different waters.

A fine piece of research on electroanalysis of metals speciation and its relevance to ecotoxicology was carried out by Morrison and Chen Wei[49]. The estimation of the potential metal detoxification capacity of the water sample, viz., complexation capacity, can be carried out through using the anodic stripping voltammetric techniques[50].

Another piece of work has been done by Matysik and Werner[51] in tears for trace metal determination by anodic stripping voltammetry. Here, microanalytical studies with injection volumes within the nanolitre range were performed and the trace metals were determined by (ASV) strongly adsorbed on the mercury electrode, thereby affecting the peak current. There was no interference from the co-existing ions and the method was applied to the analysis of environmental samples, e.g. polluted water, with recoveries of 99-103.5%.

An excellent work has been done by Prig Wu[52] on ASV of Pb(II), Cu(II) and Cd(II) using in situ-generated ultra thin mercury-films on glassy carbon disc electrode. Another piece of work has been done by D.P Lwlen[53] reported ASV at the natural pH of the sample and use of chelax ion-exchange resin and of UV irradiation technique to destroy organic matter.

In view of the problem of chemical speciation and its relationship to ecotoxicology in the natural environment, the present study is undertaken to make modest beginning in this field of research in relation to global interest.

1.7 Objective of the Research

Many metals in the ionic form have performed essential catalytic physiological functions in living systems, but in excess they can cause damage to specific organs[31]. On the other hand, metals like cadmium, mercury, lead etc. are potentially toxic when consumed even

in a very trace level. Moreover, free metal ions are more toxic than metal chelates. The chelating agents are used in medicine for the formation of soluble, easily excreatable metal chelates by sequestering metal ions in the circulation of blood. Thus the identification and quantification of metals called speciation analysis is essential to study the relationships between the various species of metals and their toxicity to specific groups of organisms.

Various electrochemical techniques are useful for studying metal speciation. Among these, cyclic voltammetry has been chosen for the present study because it is in the forefront of the study of electron transfer and its consequences. Due to the increasing development of computer controlled experienced experiments with automated data collection and due to the development of mathematical description of potentiodynamic curves this experimental method has expanded into the laboratory praxis widely in the last few decades. The present study design is implemented under computer controlled potentiostat conditions and stationary glassy carbon (GC) electrodes.

As a ligand, Catechol is an attractive choice for a number of reasons:

(i) Catechol tends to be remaining stable under considerable thermal and chemical stress. In the harsh environment of an electrocatalytic system, chemical stability is crucial.

(ii) There exists an excellent bidentate site between the two normal and/or deprotonated hydroxyl oxygens.

(iii) The hydroxyl oxygens have an acidic proton that may be removed and replaced, influencing the electron density along the phenyl ring.

(iv) Catechols produce quinones like structure.

Cu(II) and Cd(II) are logical choices for metal centers with which Catechol forms complexes of catechol because:

(i) Both Cu and Cd are mainly present as divalent ions and as metal-organic complexes in normal soil and in many estuaries.

(ii) Cu(II) (a d^9 ion) is toxic above a certain level (μg/L), while Cd(II) (a d^{10} ion) is potentially toxic at any level of concentration.

(iii) They form stable coordination complexes in aqueous medium quite easily.

(iv) Their electrochemistry is well behaved.

Thus the goal of this research project is quite straightforward. The research work involves:

(i) Cyclic voltammetric analysis to reveal the complexation capacity of metals like Cu(II) and Cd(II) with catechol, a bidentate ligand.

(ii) Job's method is an extremely versatile approach to the determination of reaction stoichiometries.

Chapter 2

2. EXPERIMENTAL

In this chapter the materials, methods and equipment used to carry out the voltammetric and spectrophotometric works are detailed. The results and discussion of these experimental study are presented separately in later chapters.

2.1 Experimental Setup

2.1.1 Voltammetric Cell

The cyclic voltammetry experiments were carried out with a Teflon capped voltammetric cell with three electrodes immersed in the aqueous solution of analyte in close proximity. The electrodes are:

(a) Glassy carbon working electrode

(b) Ag/AgCl (Satd. KCl) reference electrode

(c) A platinum wire as the counter electrode

The cell configuration and the potentiostat with computer interface are shown in Fig. 2.1.

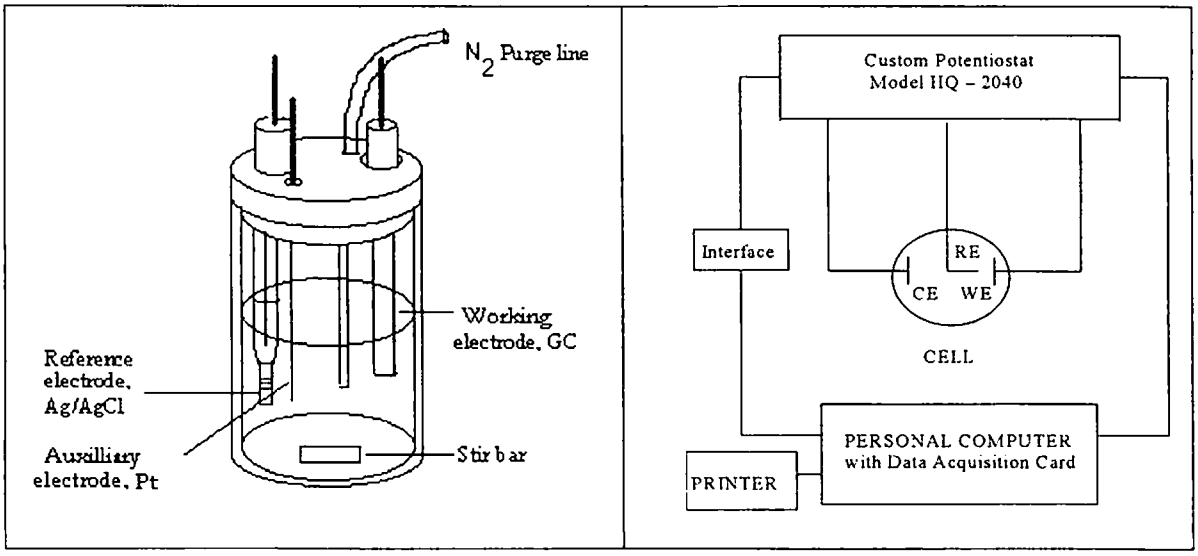

Fig 2.1 Electrochemical cell and potentiostatic setup.

1 M KCl solution is selected as the supporting electrolyte for Cu(II)-catechol and Cd(II)-catechol interaction.

2.1.2. Computer Controlled Potentiostat

The current-voltage measurement system used in this study was a custom made potentiostat Model 2040, developed by the Advanced Analytics (AA), Virginia, USA. The potentiostat voltage compliance is ± 12V and the current output of 20 mA (maximum). The maximum current sampling frequency is 170 kHz. The soft wares are written in TURBO-PASCAL language for about 17 electrochemical techniques including CV.

2.1.3. Computer Controlled Magnetic Stirrer

For the purpose of purging and mixing of the solution, a magnetic stirrer was interfaced with a 486 DX PC through a 12-bit data acquisition card from the Real Time Devices, USA. A Teflon coated magnetic bar was used as magnetic stirrer. Special software was used for switching and selecting the duration of stirring.

2.2. Operational Procedures of Computerized Electrochemical System

On power up the system, the directory must be changed to the directory in which the electrochemistry programs are saved and the potentiostat should be reset each time through the system-reset software. After reset of the potentiostat the EC batch file is to be activated for control experiments, following the menu as appears for special experiments according to the following display.

COMPUTERIZED ELECTROCHEMISTRY SYSTEM

(0) Exit – Exit to system
(1) Linear and Cyclic Voltammetry
(2) Pulse Voltammetry
(3) Chronoamperometry / Chronocoulometry
(4) Pulse Chronopotentiometry

SELECT EXPERIMENT TYPE = 1

On selection of (1) from the main menu a new menu with two options will appear:

LINEAR AND CYCLIC VOLTAMMETRY

(0) Exit- Exit to main menu
(1) LSV – Linear Scan Voltammetry

(2) CV- Cyclic Voltammetry

SELECT EXPERIMENT TYPE = 2

When option (2) from the above menu is chosen, the following menu will appear:

CYCLIC VOLTAMMETRY

Comments	=	
Stripping mode (y/n)	=	N
Initial potential (mV)	=	
Final potential (mV)	=	
Scan rate (mV/s)	=	
Number of sweeps	=	
height Step	=	
Gain (1 – 20)	=	
Initial delay	=	
Data OK (y/n)	=	Y

By providing an appropriate set of input data in the CV data entry screen, the defined experiment can be performed and progress of the whole experiment will be displayed on the monitor.

2.3. Experimental Measurements

2.3.1. Apparatus and Equipments

The following apparatus and equipment were used during the experiment:

(i) Computerized Electrochemistry system, Model HQ 2040,
(ii) Glassy carbon electrode, Ag/AgCl (satd. KCl) electrode as the reference electrode,
(iii) Platinum wire as the counter electrode,
(iv) Pyrex glass volumetric cell (10 mL),
(v) Pyrex glass micro cell with Teflon cap,
(vi) Teflon coated magnetic bar,
(vii) Pyrex glass volumetric flask (100 mL), and

(viii) Micropipette [graduating micropipette (10 μL, 20 μL with tips)]

2.3.2. Chemicals

The following analytical grade chemicals procured from different countries were used as supporting electrolyte, ligand, metal source etc.

(i) KCl (BDH, UK)
(ii) $Cu(NO_3)_2$, $3H_2O$ (MERCK, Germany)
(iii) $CdCl_2$. H_2O (MERCK, Germany)
(iv) N_2, 99.99% pure (BOC, Bangladesh)
(v) Milli-Q-water
(vi) Catechol (99.5%, Aldrich, USA)

2.3.3. Preparation of Stock Solutions

Preparation of KCl solution: A solution of 0.1 M KCl in Milli-Q-water was also prepared.

Preparation of metal solutions: Aqueous solutions of 1 mM Cu(II) and 1 mM Cd(II) was prepared using A R grade $Cu(NO_3)_2.3H_2O$ and $CdCl_2.H_2O$ in Milli-Q-water.

Preparation of catechol solutions: 0.1 M catechol solution was first prepared using 0.1 M KCl solution. From this solution, 1.0 mM, 2.0 mM, etc. catechol solution of desired strength was made with 0.1 M KCl solution.

Preparation of buffer solution: A. R. acetic acid and sodium acetate were used to prepare acetate buffer. 0.2 M solutions of CH_3COONa and CH_3COOH were made first and the required quantity of them were mixed together to obtain a buffer of 4.23 pH value. A pH-meter obtained from METTLER, TOLEDDO was used for pH measurement.

2.3.4. Preparation of the Working Electrode

The working electrode used in this study is glassy carbon electrode (GEC) procured from the Bio-analytical System (BAS), USA. This electrode preparation includes the polishing and conditioning of the electrode.

The glassy carbon electrode was polished with fine alumina powder (0.3 micron or lower)

on a wet polishing cloth. To do so a part of the cloth was made wet with deionized water and alumina powder was sprinkled on it. The glassy carbon electrode was then polished on this surface by softly pressing the electrode against the polishing surface in the end for 5 - 10 minutes. The electrode was then thoroughly washed with deionized water. At this point the electrode surface would look like a shiny black mirror.

The electrode was conditioned by running a blank CV in 1 M KCl in the potential range of -300 to +800 mV at a scan rate of 100 mV/s. This is the working potential range followed in the present study. During the process, oxidizable or reducible impurities on the electrode surface are completely converted to electroactive species.

2.3.5. Removal of Dissolved Oxygen with Pure Nitrogen

First the cell and the Teflon top (with the counter electrode) is cleaned with deionized water, any excess water is wiped off with a tissue paper. A small magnetic stir-bar is put in the cell. The cell is filled with desired volume of the analyte solution and the Teflon cap is placed on the cell. The reference electrode and the purging tube are inserted through the holes. The purging tube should be halfway inside the solution. A medium level of nitrogen (99.998% pure) flow through the solution without spilling the solution over the top is established. The purging of the analyte solution with pure nitrogen is carried out for 10 minutes to drive off dissolved oxygen.

2.3.6. Experimental procedure for Cyclic Voltammetry (CV)

In order to study the interaction of Cu(II) and Cd(II) with catechol first of all the working electrode was polished and conditioned as described before. Then a 5 mL of KCl solution, 5 mL of acetate buffer of pH 4.23, and required amount of metal/metal-catechol solution pipetted into the volumetric cell and the electrode were inserted into the electrolytic cell. Then pure N_2 was purged through the cell solution for 10 minutes to remove dissolved oxygen. In order to study the interactions of Cu(II)-catechol, and Cd(II)-catechol using cyclic voltammetry the chosen potential ranges were -700 mV to +1100 mV and -1100 mV to +1100 mV respectively.

Solutions of different metal to catechol millimolar concentrations were used to observe the CV experiments at different scan rates (25, 50, 100, 150 and 200 mVs^{-1}).

However, the following precautions must be taken into consideration to perform any electrochemical measurement successfully under potentiostatic condition.

(i) the electrodes should not be connected until the reset program run is complete,

(ii) the cell should never be disconnected while the experiment is in progress,

(iii) the computer never be turned off during an experiment,

(iv) the electrode connection should be perfect, and

(v) if the main power turns off, one should shut down the system and disconnect all electrodes quickly, also unplug the stirrer.

2.3.7 Experimental Procedure for Chronocoulometry (CC)

Chronocoulometric experiments have been done using the same solution and electrochemical setup used for cyclic voltammetry. The experiment started at a potential (initial E) at which there is no electrolysis. The potential is then changed instantaneously to a value that leads to oxidation or reduction of electroactive species in solution (Final step E) and is held at the potential for a definite time period (250 ms). The potential is stepped to a third potential at which the species formed on the first step is re-electrolyzed. The first and the second potential steps are also referred to as the forward and reverse potential steps respectively. The background voltammogram is obtained by performing CC of the supporting electrolyte. The excitation potential was decided by performing CV of the corresponding analyte. The chronocoulometry of metal ions, ligand and metal-ligand solutions are carried out at 1.00×10^{-3} M concentration. The working electrode is subjected to forward and reverse potential steps and a typical chronocoulogram is recorded.

2.4 Spectrophotometric Analysis

2.4.1 Spectrophotometer

A double beam UV-Visible recording spectrophotometer, Model UV-160 A, Shimadzu (Japan), in the wavelength range 200 – 1100 nm was used in this experiment. In a double beam instrument, radiation from the filter or monochromator is split into two beams that simultaneously pass through the reference and sample cells before striking two matched photodetectors. The two outputs are amplified, and their ratio, or the log of their ratio, is obtained electronically or computed and displayed on the output device.

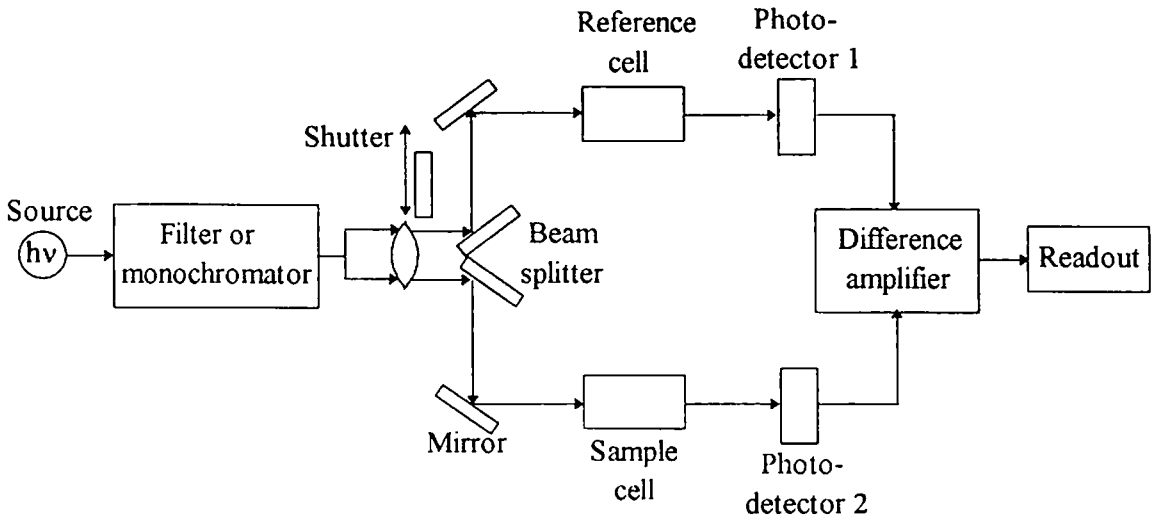

Fig. 2.2 A double-beam-in-space spectrophotometer.

Double beam instruments offer the advantage that they compensate for all but the most short-term fluctuations in the radiant output of the source. They also compensate for wide variations of source intensity with wavelength. Furthermore, the double-beam design is well suited for continuous recording of absorption spectra.

2.4.2 *Experimental procedure*

Aqueous solutions of metal ions, Cu(II) and Cd(II), and catechol of desired concentrations were prepared. They were buffered to pH 4.23. The resulting metal and catechol solutions were then mixed in the following proportion so that the total molar concentration remains constant.

M(II) mmol x 10^{-4}	1	2	3	4	5	6	7	8	9
Catechol mmol x 10^{-4}	9	8	7	6	5	4	3	2	1

The UV-spectrum of each solution was scanned in the wavelength range between 200 and 400 nm, and the absorbance of each solution at 222 nm was obtained. A plot of absorbance versus the mole fraction of catechol showed two linear branches: one when catechol is the limiting reagent and a second when the metal is the limiting reagent. The intersection of these two branches occurs when a stoichiometric mixing of metal and catechol is reached. The mole fraction of catechol at this intersection is used to determine the value of n for the metal-catechol complex, ML_n.

$n = n_L/n_M = X_L/X_M = X_L/(1 - X_L)$

Several precautionary measurements were taken.

(i) Plots of absorbance versus X_L were constructed for several different wavelengths and for several different values of n_{total}. Since the maximum absorbance occurs at the same value of X_L for each set of conditions, suggesting a single metal-catechol complex being formed.

(ii) The metal-catechol complex was found to obey Beer-Lambert's law ($A = \varepsilon cl$, where A is the absorbance, ε is the molar absorptivity in L mol^{-1} cm^{-1}, c is the concentration of the absorbing species in g L^{-1} and l is the cell length in cm) for the range of concentrations used in constructing the plot of absorbance versus X_L.

(iii) The plot of absorbance versus X_L revealed a V-shaped curve (i.e. no significant curvature) indicating that the formation constant of metal-catechol is expectedly large.

Chapter 3

Data Analysis and Results

3.1 General

The following parameters from voltammetric experiments are used for calculations:

1) Cathodic peak current (I_{pc})

2) Anodic peak current (I_{pa})

3) Cathodic peak potential (E_{pc})

4) Anodic peak potential (E_{pa})

5) Peak potential difference (ΔE_p)

6) Current function ($I_{pc}/v^{1/2}$)

7) Cathodic and anodic current ratio (I_{pa}/ I_{pc})

3.2 Cyclic voltammetry

The peak currents (I_{pa} and I_{pc}) and the peak potentials obtained by using the data of the figures .

Peak potential differences (ΔE_p), the current functions ($I_{pc}/v^{1/2}$) and the cathodic to anodic peak current ratio (I_{pa}/ I_{pc}) are calculated and presented in table.

The heterogeneous charge transfer rate constant k_f, for reversible and irreversible systems are calculated by using equations (32) and (52) respectively. The results are tabulated in tables (2-30).

A typical calculation for charge transfer rate constant is given below:

3.2.1 Reversible system

The peak current related to the charge transfer rate constant, k_f, for the reaction

$$Cd(II) + Cat. \longrightarrow Cd(II)\text{-}Cat.$$

is given by the following equation

$$i_{pc} = nFAC_0^o k_f$$

Where, i_{pc} = cathodic peak current = 7.32×10^{-6} A at scan rate 25 mV/s

n = no. of electrons involved in the reaction =2

F= 96500 coulombs

A = area of the electrode = 0.05 cm^2

$C^0_{ox} = 1.00 \times 10^{-6}$mol/L

The charge transfer rate constant for this reaction is

$$k_f = 7.85 \times 10^{-4}\text{cm/S}.$$

In this way reversible charge transfer rate constants at various concentration and scan rates are calculated. The results are shown in tables.

3.2.2 Irreversible system

Cu (II) gives two pairs of peak in the voltammogram corresponds to the following reactions

$$Cu^{2+} \xrightarrow{+e} Cu^{+} \xrightarrow{+e} Cu^{0} \quad \text{(Reduction process)}$$

$$Cu^{0} \xrightarrow{-e} Cu^{+} \xrightarrow{-e} Cu^{2+} \quad \text{(Oxidation process)}$$

The charge transfer rate constant for this irreversible process is calculated on the basis of following equation

$$E_{pc} = E_{1/2} - b\left[0.52 - \frac{1}{2}\log\frac{b}{D} - \log k_f + \frac{1}{2}\log\nu\right]$$

Where

E_{pc} = cathodic peak potential =0.199volt

b = peak potential in terms of Tafel slope = $\dfrac{2.303RT}{\alpha n_\alpha F}$

$E_{p/2}$ = half wave potential calculated from the equation

$$E_{pc} = E_{p/2} - \frac{1.857RT}{\alpha n_\alpha F}$$

α = transfer co-efficient

n_α = no. of electrons involved in the rate determining step.

$$(E_{pc})_2 - (E_{pc})_1 = \frac{RT}{\alpha n_\alpha F} \ln \sqrt{\frac{\nu_1}{\nu_2}}$$

$$-0.1999 + 0.1933 = \frac{8.314 \times 298}{\alpha n_\alpha \times 96500} \ln \sqrt{\frac{0.025}{0.050}}$$

$$-0.0066 = \frac{0.0257}{\alpha n_\alpha} \ln(0.3466)$$

$$\alpha n_\alpha = 1.350$$

$$b = \frac{2.303RT}{\alpha n_\alpha F}$$

$$= \frac{2.303 \times 8.314 \times 298}{1.350 \times 96500}$$

$$= 0.044$$

$$E_{1/2} = -0.1933 + \frac{1.857RT}{\alpha n_a F}$$

$$= -0.1933 + \frac{1.857 \times 8.314 \times 298}{1.350 \times 96500}$$

$$= -0.1933 + 0.035$$

$$= -0.158$$

Diffusion co-efficient for the irreversible process is calculated by the following equation

$$i_{pc} = 2.99 \times 10^5 \times n \times (\alpha n_a)^{1/2} A D^{1/2} C \nu^{1/2}$$

$$4.81 \times 10^{-6} = 2.99 \times 10^5 \times 2 \times 1.16 \times 0.05 \times D^{1/2} \times 1 \times 10^{-6} \times 0.158$$

$$D = 0.308 \times 10^{-5} cm^2 / S.$$

Charge transfer rate constant for this system is calculated as follows

$$-0.1933 = -0.158 - 0.044 \left(0.52 - \frac{1}{2} \log \frac{0.044}{0.308 \times 10^{-5}} - \log k_f + \frac{1}{2} \log \nu\right.$$

$-0.0353 = -0.044(0.52 - 2.077 - \log k_f - 0.801)$

$0.802 = -\log k_f - 2.358$

$\log k_f = -3.16$

$k_f = 6.92 \times 10^{-4}$ cm/S.

The charge transfer rate constant values for different irreversible systems are calculated and tabulated in the table.

3.3 Chronocoulometry *(CC)*

Diffusion coefficient (D), area of the electrode (A) and no. of electrons in the reaction are calculated using chronocoulometry. The equation used for this purpose is

$$Q_{total} = \frac{2nFAC^o_{ox}D_o t^{1/2}}{\pi^{1/2}} + nFA\Gamma_o + Q_{dl} \qquad (3.3.1)$$

Where, Γ_0 = Surface excess.

Q_{dl} = Double layer charge obtained from the chronocoulogram of the supporting electrolyte.

A plot of Q_{total} *vs.* $t^{1/2}$ gives a straight line with slope = $\frac{2nFAC^o_{ox}D}{\pi^{1/2}}$

Diffusion coefficient is calculated from the value of the slope.

For adsorption study Q_{total} *vs.* $t^{1/2}$ and Q_r *vs.* Θ are plotted and are presented in figure. For different systems Q_r can be calculated by using the equation

$$Q_r = Q_\tau - Q\ (t > \tau)$$

And Θ can be calculated by using equation

$$\Theta = [\tau^{1/2} - (t-\tau)^{1/2} - t^{1/2}]$$

Charge transfer rate constant k_f is calculated according to the following equation

$$k_f = \frac{slope \times H \times \pi^{1/2}}{2 \times nFAC_0^o}$$

$$H = \frac{\pi^{1/2}}{2 \times t_i^{1/2}}$$

$$= \frac{3.14}{2 \times 2.8}$$

$$= 0.561$$

$$= \frac{12.411 \times 0.561 \times 3.14}{2 \times 2 \times 1.3 \times 96500 \times 0.05 \times 10^{-3}}$$

$$= \frac{12.4112 \times 0.561 \times 3.14}{25090 \times 10^{-3}}$$
$$= 0.871$$

The values of Q_{total}, Q_r, τ and Θ are calculated and are tabulated in the tables.

Chapter 4

4. Results and Discussions

4.1. Cyclic Voltammetric Observations

The redox behavior of copper(II) and copper(II)-catechol, cadmium(II) and cadmium(II)-catechol in 0.1 M KCl solution were studied at various scan rates at room temperature using cyclic voltammetric technique at glassy carbon electrode (GCE). In each case, the pH of the solution was kept constant at 4.23 with an acetate buffer.

4.1.1. Cyclic Voltammetry of Catechol in 0.1M KCl at GCE

It was reported earlier[55] that catechol and/or its oxidation product has significant interaction with the electrode surface. As a result, there is a possibility of adsorbed species would undergo electron transfer processes and generate charge selective active sites that causes some change in the surface properties of the electrode. That is why analysis of the electrochemistry of catechol is so complicated.

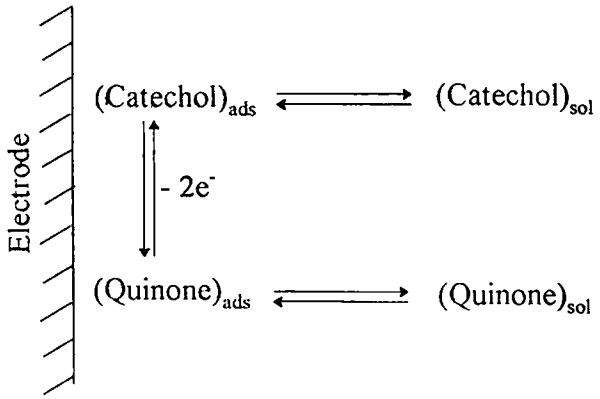

Scheme 1 Electrochemistry of Catechol at the electrode surface

Fig. 4.1 shows a cyclic voltammogram of 1 mM catechol in 0.1 M KCl at a scan rate of 100 mVs^{-1} in the potential window –700 mV to +1100 mV.

The voltammogram shows two prominent peaks - one cathodic and one anodic at -45 mV and +650 mV respectively. Two very minor peaks of shouldering in nature, cathodic at +500 mV and anodic at +100 mV are also observed, and found unchanged in heights with the variation of scan rates.

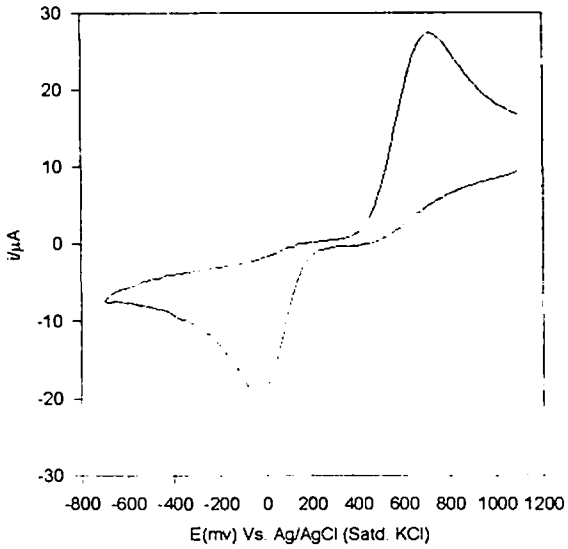

Fig. 4.1 Cyclic voltammogram of 1 mM Catechol in 0.1 M KCl at 100 mVs^{-1} scan rate.

These four peaks correspond to two, one electron components of the overall two-electron process:

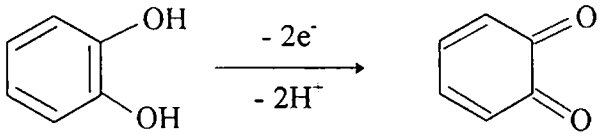

These steps become more prominent if the CV of catechol is running after 15 - 20 minutes electrode activation at $150mVs^{-1}$. The peak potentials are broad, and widely separated. The two one-electron oxidations are according to **Scheme 2.** However, on the fully activated electrode, the wave shape approaches the expected for an overall two-electron process where the intermediate oxidation state is unstable with respect to disproportionation, and the electrode processes involved are kinetically facile[56]. The quinone product of the two-electron oxidation of catechol is stable on the cyclic voltammetric time-scale.

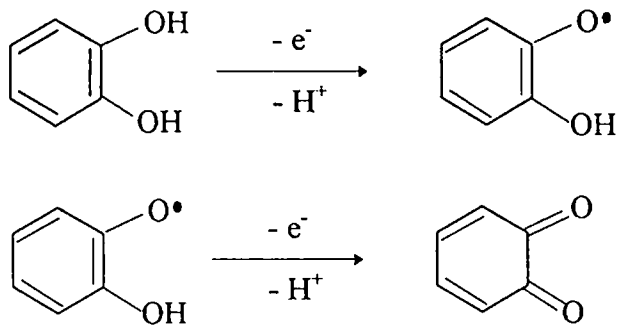

Scheme 2 Proposed redox mechanism for catechol

The wave shape for the second oxidation and reduction steps is similar to that expected for a reversible one-electron couple.

The voltammograms of catechol in 0.1 M KCl at different scan rates (25, 50, 100, 150 and 200 mVs^{-1}) are shown in Fig. 4.2. The current voltage data and the derived parameters such as anodic to cathodic current ratio and current functions ($i_p/v^{1/2}$) are compiled in **Table 4.1(a)** and **4.1(b)**.

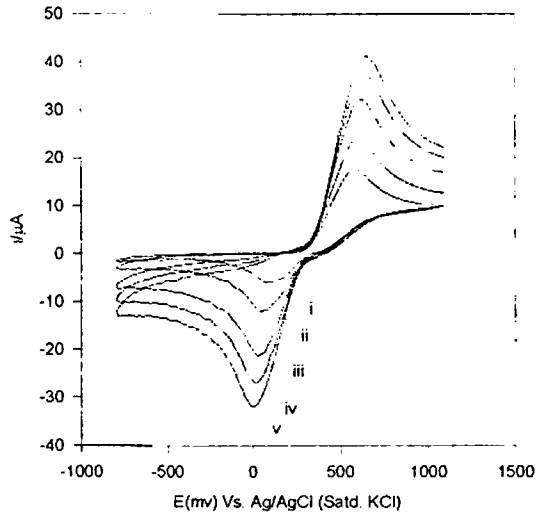

Fig. 4.2 Cyclic voltammogram of 1 mM Catechol in 0.1 M KCl at (i) 25, (ii) 50, (iii) 100, (iv) 150 and (v) 200 mVs^{-1} scan rates.

Another notable observation is that although the peak current of both i_{pc2} and i_{pa2} varies linearly with scan rate (Fig. 4.3) and both passes through the origin. However, chronocoulometry results show that the charge vs. $(time)^{1/2}$ plot cuts the $(time)^{1/2}$ axis

with an intercept. Transformation of catechol to quinone which is likely to adsorb on the electrode surface. Thus our results are very much similar to the observations reported by Chambers[57].

Table 4.1(a) Current-Potential data of 1 mM Catechol in 0.1 M KCl at various scan rates.

Scan Rate (mVs^{-1})	Anodic Peak Current, i_{pa} (+)(μA)	Cathodic Peak Current, i_{pc} (-) (μA)	Anodic Peak Potential, E_{pa} (+)(mV)	Cathodic Peak Potential, E_{pc} (-) (mV)
25	10.25	5.72	641.18	23.53
50	16.10	10.00	670.59	41.18
100	22.91	16.36	688.83	52.94
150	25.35	18.74	733.54	94.12
200	27.61	21.90	756.77	111.77

Table 4.1(b) Derived parameters obtained from the current-voltage data.

Scan Rate (mVs^{-1})	$\Delta E = E_{pa} - E_{pc}$ (mV)	i_{pa}/ i_{pc}	$i_{pc}/ \nu^{1/2}$ (μAs^{-1})	$k_f \times 10^{-4}$
25	617.65	1.79	1.14	8.13
50	629.42	1.61	1.41	14.16
100	635.89	1.40	1.64	23.28
150	639.42	1.35	1.53	26.73
200	645.00	1.26	1.26	32.73

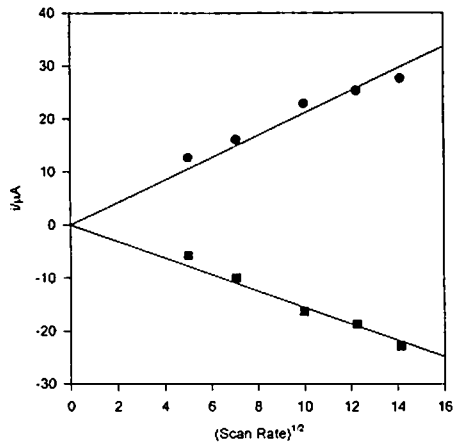

Fig. 4.3 Plots of peak current, i_p vs. square root of scan rate, $\nu^{1/2}$ for Catechol.

This suggests that the redox behavior of catechol at glassy carbon electrode (GCE) is controlled both by diffusion and adsorption processes. This also confirms the transformation of Catechol to quinine which is likely to adsorb on the electrode surface. The voltammogram of Catechol in 0.1 M KCl at different concentrations were also studied (**Fig. 4.4**) and the results are tabulated in **Table 4.2(a)** and **4.2(b)**.

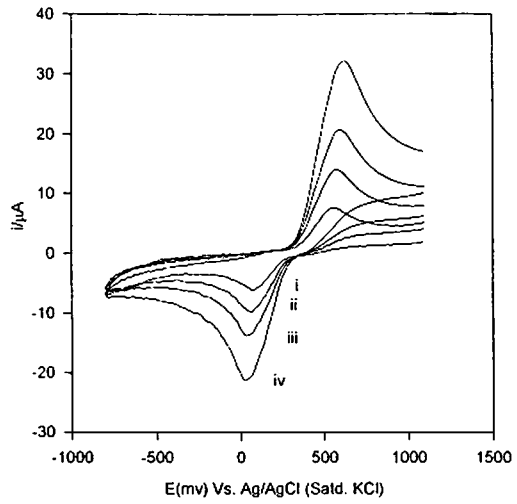

Fig. 4.4 Cyclic voltammogram of 1 mM Catechol in 0.1 M KCl at various concentrations (i) 0.2, (ii) 0.4, (iii) 0.6, (iv) 0.8 and (v) 1 mM at a scan rate of 100 mVs^{-1}.

Table 4.2(a) Current-Potential data of 1 mM Catechol in 0.1 M KCl at various concentrations.

Concentrations (mM)	Anodic Peak Current, i_{pa} (+)(μA)	Cathodic Peak Current, i_{pc} (-)(μA)	Anodic Peak Potential, E_{pa} (+)(mV)	Cathodic Peak Potential, E_{pc} (+) (mV)
0.2	6.26	4.64	530.77	76.92
0.4	12.13	7.45	530.77	61.54
0.6	17.37	10.13	561.54	61.54
0.8	23.13	14.06	569.23	61.54
1.0	26.67	17.50	567.16	52.24

Table 4.2(b) Derived parameters obtained from current-potential data.

Concentrations (mM)	$\Delta E = E_{pa} - E_{pc}$ (mV)	i_{pa}/ i_{pc}	$i_{pc}/ \nu^{1/2}$ (μAs^{-1})
0.2	453.85	1.35	0.46
0.4	469.23	1.63	0.74
0.6	500.00	1.71	1.01
0.8	507.69	1.64	1.41
1.0	514.92	1.53	1.75

4.1.2 Cyclic Voltammetry of Cu(II) in 0.1 M KCl at GCE

The redox behavior of Cu(II) solution was studied at pH 4.23 at a GCE in 0.1 M KCl at room temperature within the potential window of -700 to +1000 mV at different scan rates and concentrations. The blank voltammogram showed no peak indicating the absence of any adsorbed electroactive species on the surface of the electrode that could undergo redox reaction within the mentioned potential window.

Fig. 4.5 shows the voltammogram of Cu(II) solution at a scan rate of 100 mVs^{-1}.

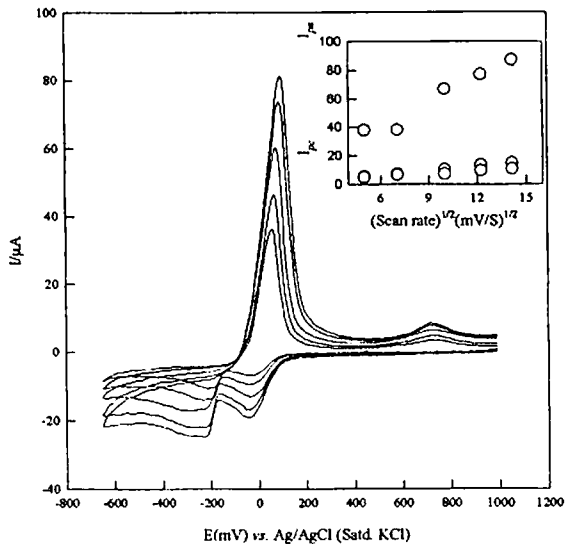

Fig. 4.6 Cyclic voltammogram of 1mM Cu(II) in 0.1 M KCl at various scan rates (25, 50, 100, 150 and 200 mVs^{-1}).

In general, increasing the scan rate is equivalent to increasing the rate of diffusion of R from the electrode (for a reductive, $O + e^- = R$, process). At faster scan rates, steeper concentration gradients are produced, increasing the rate of diffusion.

Table 4.3(a) Current-Potential data of 1 mM Cu(II) in 0.1 M KCl at different scan rates.

Scan Rate (mVs^{-1})	Anodic Peak Current, i_{pa} (μA)		Cathodic Peak Current, i_{pc} (μA)		Anodic Peak Potential, E_{pa} (mV)		Cathodic Peak Potential, E_{pc} (mV)	
	1 (+)	2 (+)	1 (-)	2 (-)	1 (+)	2 (+)	1 (-)	2 (-)
25	2.50	37.92	5.20	4.81	753.33	26.67	26.67	193.33
50	3.25	38.12	7.00	6.50	733.33	66.67	28.82	199.99
100	4.70	66.64	10.19	7.06	726.66	46.67	32.74	253.33
150	5.49	76.83	13.33	9.41	720.00	26.67	46.32	259.99
200	5.78	87.12	14.67	10.67	726.66	60.00	53.33	262.67

Table 4.3(b): Derived parameters obtained from current-potential data.

Scan Rate (mVs^{-1})	$\Delta E = Ep_a - Ep_c$ (mV)		ip_a / ip_c		$ip_c / v^{1/2}$ (μAs^{-1})		$k_f \times 10^{-4}$	
	1	2	1	2	1	2	1	2
25	780.00	220.0	0.481	7.88	1.04	0.96	0.0047	6.92
50	762.15	266.66	0.464	5.86	0.99	0.92	9.77	9.23
100	759.40	300.00	0.461	9.44	1.02	0.71	14.45	10.0
150	766.31	286.66	0.412	8.16	1.09	0.77	19.05	13.06
200	779.99	322.66	0.374	8.16	1.04	0.75	20.89	15.14

R will diffuse away from the electrode faster as the scan rate is increased. The diffusion of R away from the electrode is a process that competes with the oxidation of R. Thus for the E mechanism, the greatest reversibility and least distortions are observed at slow scan rates. Away from reversibility becomes greater and greater with increasing scan rates. There is no exception in the studied case. The diffusion of oxidized and reduced forms of the Cu(II)/Cu(I) and Cu(I)/Cu(0) couples is shown schematically in **Fig. 4.7**.

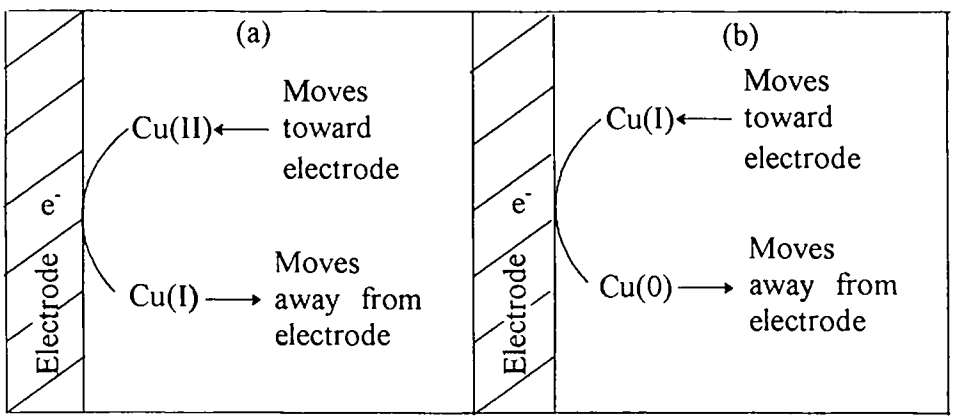

Fig. 4.7 Schematic diagram showing (a) transport of Cu(II) toward the electrode and Cu(I) away from the electrode (b) transport of Cu(I) toward the electrode and Cu(0) away from the electrode following the reduction of Cu(II).

In fact the E mechanism of copper more generally as follows:

$Cu(II)_{sur} + e^- \rightleftharpoons Cu(I)_{sur}$

$Cu(I)_{sur} \rightarrow Cu(I)_{sol}$

And

$Cu(I)_{sur} + e^- \rightleftharpoons Cu(0)_{sur}$

$Cu(0)_{sur} \rightarrow Cu(0)_{sol}$

It is also observed that the difference Δi_p, of the cathodic and anodic peak current is large and increases with increasing scan rate.

Fig. 4.8 shows a plot of peak current, i vs. square root of scan rate, $\nu^{1/2}$. The peak current variation with $\nu^{1/2}$ is linear suggesting diffusion controlled redox processes, that is, the rate of electron transfer is controlled by the rate of supply of material to the electrode by diffusion.

The ratio of the peaks i_{pa1} and i_{pc1} is slightly greater than unity while that of i_{pa2} and i_{pc2} is nearly unity. Thus the peaks associated with the both redox couple, Cu(II)/Cu(I) and Cu(0)/Cu(I), are conforming a single, reversible, electron transfer mechanism. Cyclic voltammograms of Cu(II) at different concentrations (0.2, 0.4, 0.6, 0.8 and 1 mM) in 0.1 M KCl at a scant rate of 100 mVs^{-1} are also recorded (**Fig. 4.9**) and the results are gathered in **Table 4.4(a)** and **4.4(b)**.

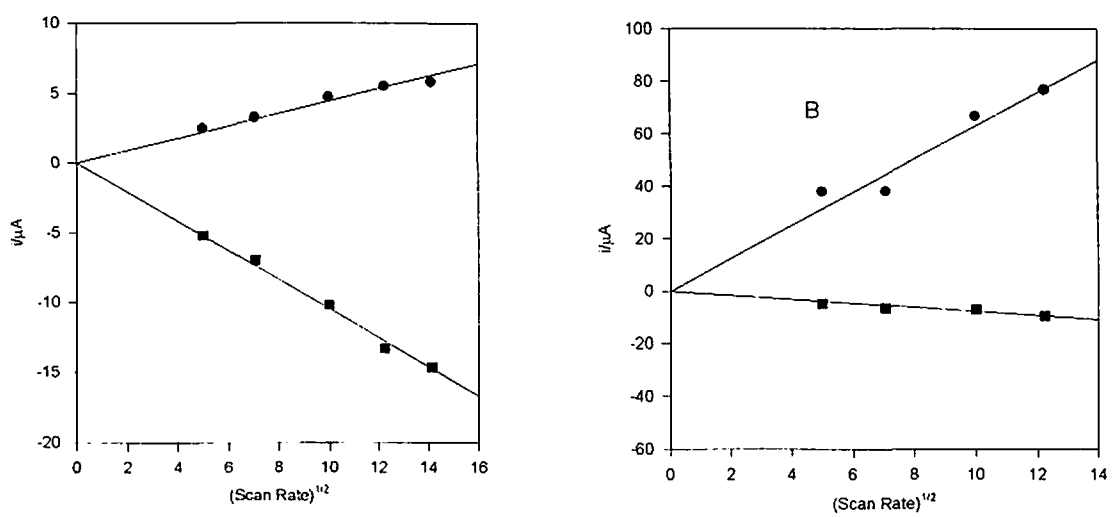

Fig. 4.8 Plots of peak current, i_p vs. square root of scan rate, $\nu^{1/2}$ for Cu(II); (A) i_{pa1} and i_{pc1} vs. $\nu^{1/2}$ and (B) i_{pa2} and i_{pc2} vs. $\nu^{1/2}$.

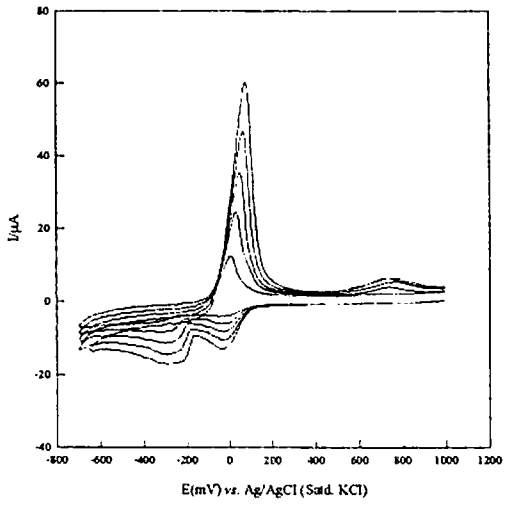

Fig. 4.9 Cyclic voltammogram of Cu(II) at various concentrations (0.2, 0.4, 0.6, 0.8 and 1 mM) solution in 0.1 M KCl at 100 mVs^{-1} scan rate.

Table 4.4(a) Current-Potential data of 1 mM Cu(II) in 0.1 M KCl at different concentrations.

Conc. (mM)	Anodic Peak Current, i_{pa} (μA)		Cathodic Peak Current, i_{pc} (μA)		Anodic Peak Potential, E_{pa} (mV)		Cathodic Peak Potential, E_{pc} (mV)	
	1 (+)	2 (+)	1 (-)	2 (-)	1 (+)	2 (-)	1 (-)	2 (-)
0.2	0.66	12.13	5.16	1.31	726.66	13.33	46.67	393.33
0.4	2.15	25.71	4.14	3.29	753.33	26.67	46.67	306.66
0.6	3.34	37.26	6.86	5.10	673.33	13.33	46.67	286.66
0.8	4.09	49.09	8.86	6.59	740.00	46.67	33.33	280.00
1.0	5.10	65.49	9.80	8.63	713.33	60.00	46.67	273.33

The entire mechanism could be formulated as follows:

$$\mathrm{Cu(II)} \underset{(i_{pa1})}{\overset{(i_{pc1})}{\rightleftharpoons}} \mathrm{Cu(I)} \underset{(i_{pa2})}{\overset{(i_{pc2})}{\rightleftharpoons}} \mathrm{Cu(0)}$$

Scheme 3 Redox mechanism of copper at the electrode surface.

Table 4.4(b) Derived parameters obtained from current-voltage data.

Concentrations (mM)	$\Delta E = E_{pa} - E_{pc}$ (mV)		i_{pa}/ i_{pc}		$i_{pc}/ \nu^{1/2}$ (μAs^{-1})	
	1	2	1	2	1	2
0.2	773.33	406.66	0.13	9.25	0.52	0.13
0.4	800.00	333.33	0.52	7.83	0.41	0.33
0.6	720.00	300.00	0.49	7.31	0.69	0.51
0.8	773.33	326.66	0.46	7.45	0.89	0.66
1.0	760.00	333.33	0.52	7.59	0.98	0.86

4.1.3 Cyclic Voltammetry of Cu(II) in Presence of Catechol at GCE

The electrochemical behavior of Cu(II) in presence of catechol in 0.1 M KCl in buffer of pH 4.23 solution has been studied using cyclic voltammetry. The cyclic voltammogram of Cu(II) solution in 0.1 M KCl in presence of catechol at 100 mVs^{-1} scan rate is shown in the **Fig. 4.10**. The voltammogram exhibits two cathodic peaks i_{pc1} and i_{pc2} are at +229.6 and -37.0 mV respectively. Obviously, the presence of catechol affects the peak potentials of Cu(II) and becomes apparent if a CV of free Cu(II) is placed over CV of Cu(II) plus catechol obtained under the similar experimental condition, shown in **Fig. 4.12**.

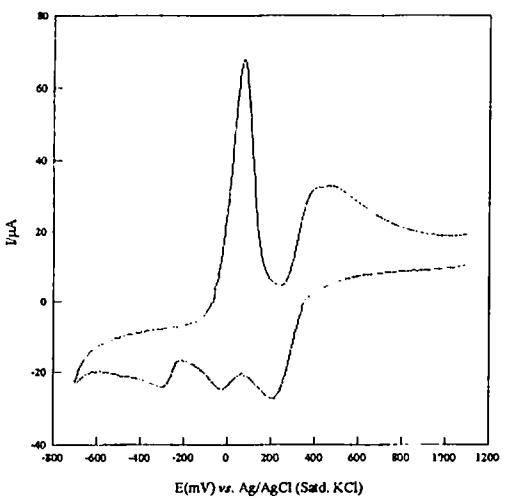

Fig. 4.10 Cyclic voltammogram of Cu(II)-Catechol in 0.1 KCl solution at a scan rate of 100 mVs^{-1}.

Both the cathodic peaks are shifted significantly towards the positive potential but the anodic peaks are shifted towards a negative potential, and the peak heights are reduced. Large shifting of the cathodic peaks (Δi_{pc1} = 257.2 mV, Δi_{pc2} = 216 mV may be explained in terms of strong participation of copper in the complex formation reaction with catechol which makes the reduction processes more difficult. The anodic peaks at +385.1 and +74.1 mV in the voltammogram are associated with the oxidation processes of copper, shifted towards a negative potential indicated that oxidation of copper has been facilitated in the presence of catechol.

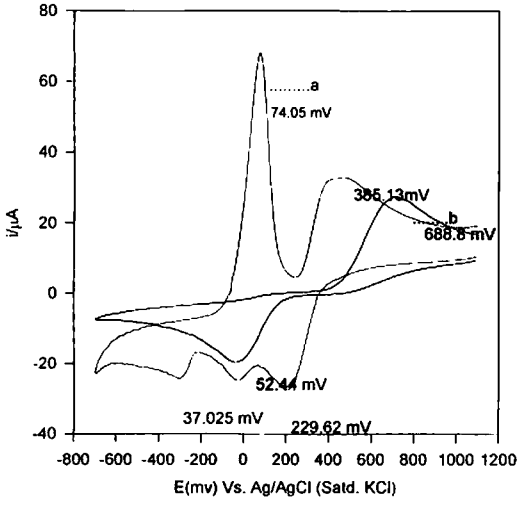

Fig. 4.11 Cyclic voltammogram of (a) Cu(II)-Catechol (1: 1 molar ratio), and (b) 1 mM Catechol in 0.1 KCl solution at a scan rate of 100 mVs^{-1}.

This is expected, because copper with higher oxidation state has more tendencies to participate in complexation reaction than that of lower oxidation state. In other words,

$$\text{Cu(II)-Cat} + e^- \xrightarrow{k_1} \text{Cu(I)-Cat}$$

$$\text{Cu(I)-Cat} + e^- \xrightarrow{k_2} \text{Cu(0)-Cat} \qquad k_1 < k_2$$

$$\text{Cu(0)-Cat} - e^- \xrightarrow{k_2'} \text{Cu(I)-Cat}$$

$$\text{Cu(I)-Cat} - e^- \xrightarrow{k_1'} \text{Cu(II)-Cat} \qquad k_1' > k_2'$$

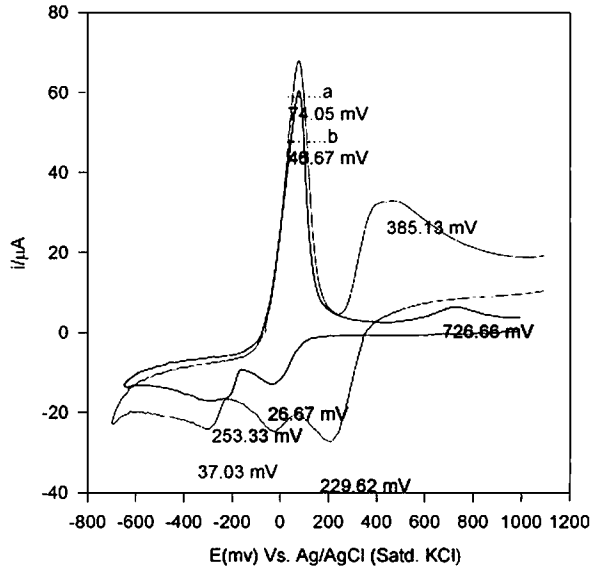

Fig. 4.12 Cyclic voltammogram of (a) Cu(II)-Catechol complex (1:1 molar ratio), and (b) 1 mM Cu(II) in 0.1 M KCl solution at a scan rate of 100 mVs^{-1}.

Cyclic voltammograms of Cu(II)-catechol solution at scan rates of 25, 50, 100, 150 and 200 mVs^{-1} are studied and given in **Fig. 4.13** and their corresponding results are compiled in **Table 4.5(a)** and **4.5(b)**. Both anodic and cathodic peak currents increase with increasing scan rates.

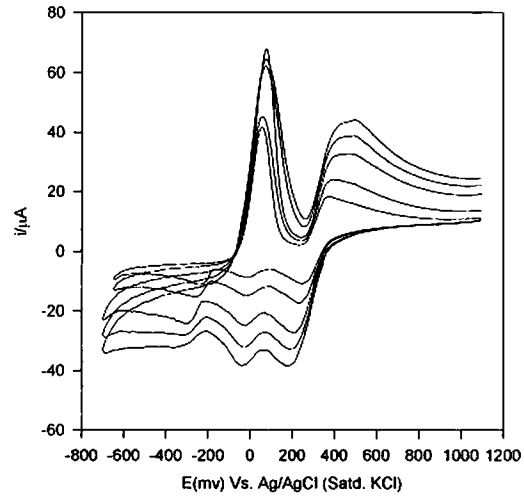

Fig. 4.13 Cyclic voltammogram of Cu-Catechol in KCl solution at different scan rates (25, 50, 100, 150 and 200 mVs^{-1}).

Table 4.5(a) Current-Potential data of Cu(II)-Catechol in 0.1 M KCl at different scan rates.

Scan Rate (mVs^{-1})	Anodic Peak Current, i_{pa} (μA)			Cathodic Peak Current, i_{pc} (μA)			Anodic Peak Potential, E_{pa} (mV)			Cathodic Peak Potential, E_{pc} (mV)		
	1	2	3	1	2	3	1 (+)	2 (-)	3	1 (+)	2 (-)	3 (-)
25	12.73	45.45	-	11.82	2.50	4.50	387.05	51.60	-	270.95	34.70	252.0
50	18.98	50.27	-	17.96	3.85	4.87	361.25	38.70	-	245.15	36.20	271.0
100	27.27	70.91	-	24.55	5.00	5.20	385.13	74.05	-	229.62	40.05	304.0
150	29.79	72.91	-	29.01	5.50	5.50	393.50	83.85	-	212.90	45.15	316.0
200	32.72	84.54	-	32.72	6.45	5.90	412.90	45.15	-	145.20	51.60	355.0

Table 4.5(b) Derived parameters obtained from current-potential data.

Scan Rate (mVs^{-1})	$\Delta E = E_{pa} - E_{pc}$ (mV)			i_{pa}/ i_{pc}			$ip_c/ \nu^{1/2}$ (μAs^{-1})			$k_f \times 10^{-4}$		
	1	2	3	1	2	3	1	2	3	1	2	3
25	116.10	86.30	-	1.08	18.25	-	2.36	0.50	0.90	16.59	3.55	6.37
50	116.10	74.90	-	1.06	13.06	-	2.54	0.54	0.68	25.41	5.62	6.95
100	155.51	114.10	-	1.11	14.20	-	2.45	0.50	0.52	34.98	7.08	7.50
150	180.60	129.00	-	1.03	13.26	-	2.37	0.45	0.45	40.74	7.85	7.76
200	267.70	96.75	-	1.00	15.51	-	2.31	0.39	0.42	46.56	9.77	8.32

The linear variation of peak current with square root of scan rate is shown in Fig. 4.14. It also evident here that with increase of scan rate, the peak current function increases suggesting both the electrode reaction and adsorption process take place simultaneously.

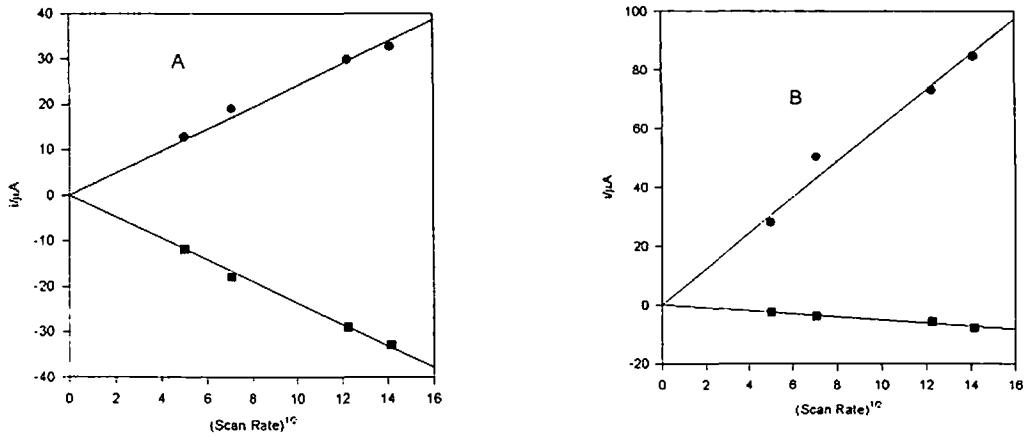

Fig. 4.14 Plots of peak current, i_p vs. square root of scan rate, $\nu^{1/2}$ for Cu(II)-Catechol; (A) i_{pa1} and i_{pc1} vs. $\nu^{1/2}$ and (B) i_{pa2} and i_{pc2} vs. $\nu^{1/2}$.

The voltammograms of three different Cu(II) to catechol molar ratio (1:1, 1:2 and 1:3) in 0.1 M KCl at different scan rates are also studied. They are very similar in shape except that in solution having 1:2 and 1:3 metal to catechol molar ratio the cathodic peak current (i_{pc1}) is decreased in comparison with that of 1:1 ratio.

Cyclic voltammograms of Cu-Catechol at different concentrations (0.2, 0.4, 0.6, 0.8 and 1 mM) solution in 0.1 M KCl at 100 mVs^{-1} are also studied (Fig. 4.15) and their corresponding current potential values are tabulated in **Tables 4.6(a)** and **4.6(b)** for comparison.

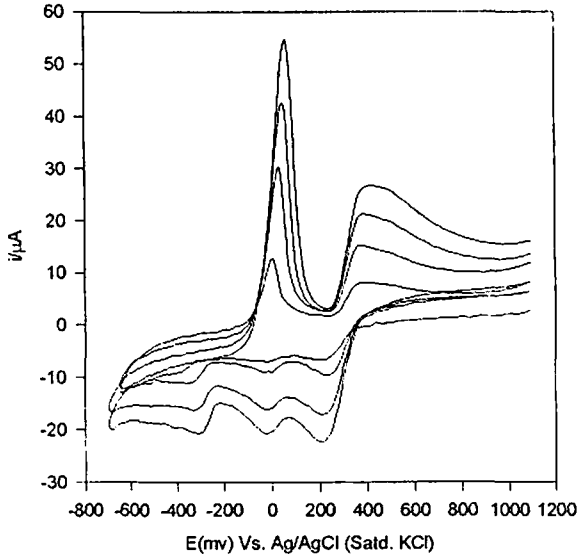

Fig. 4.15 Cyclic voltammogram of Cu-Catechol (1:1 molar ratio) at different concentrations (0.2, 0.4, 0.6, 0.8 and 1 mM) in 0.1 M KCl solution at 100 mVs^{-1} scan rate.

Table 4.6(a) Current-Potential data of Cu(II)-Catechol system at various concentrations (0.2, 0.4, 0.6, 0.8 and 1 mM) in 0.1 M KCl solution at GCE with scan rate of 100 mVs^{-1} at pH 4.23 at 25^0C.

Conc. (mM)	Anodic Peak Current, ip_a (μA)			Cathodic Peak Current, i_{pc} (μA)			Anodic Peak Potential, E_{pa} (mV)			Cathodic Peak Potential, E_{pc} (mV)		
	1	2	3	1	2	3	1	2	3	1 (-)	2 (-)	3 (-)
0.2	6.08	13.73	-	4.90	1.08	1.96	366.66	33.33	-	213.33	39.99	226.6
0.4	11.37	32.73	-	8.23	2.74	3.72	253.33	60.00	-	253.33	26.66	273.3
0.6	18.21	44.63	-	16.16	3.59	4.62	360.00	33.33	-	233.33	33.33	326.6
0.8	23.41	57.67	-	20.84	4.00	5.71	233.33	60.00	-	226.66	39.99	306.6
1.0	30.18	74.48	-	22.34	6.27	7.84	373.33	86.66	-	233.33	39.99	299.9

Table 4.6(b): Derived parameters obtained from current-potential data.

Conc. (mM)	$\Delta E = E_{pa} - E_{pc}$ (mV)		i_{pa}/ i_{pc}		$i_{pc}/ \nu^{1/2}$ (μAs^{-1})		
	1	2	1	2	1	2	3
0.2	580.00	73.33	1.24	12.73	0.49	0.11	0.19
0.4	506.66	86.66	1.38	11.93	0.82	0.28	0.37
0.6	593.33	66.67	1.13	12.43	1.62	0.36	0.46
0.8	460.00	100.00	1.12	14.43	2.08	0.40	0.57
1.0	606.66	126.66	1.35	11.88	2.23	0.63	0.63

From the above observations it is concluded that Cu(II)-catechol complex was formed in the experimental condition. And the tendency of complex formation increases with increasing catechol concentration.

4.1.4 Cyclic Voltammetry of Cd(II) in 0.1 M KCl at GCE

The redox behavior of Cd(II) solution was studied at GCE in 0.1 M KCl at pH 4.23 at room temperature within the potential window of -1100 to +800 mV at different scan rates. A blank voltammogram was taken and showed no peaks indicating the absence of any electroactive species on the surface of the electrode that could interfere within the mentioned potential window.

The voltammetric response of Cd(II) solution in 0.1 M KCl solution with scan rate of 100 mVs^{-1} is illustrated in **Fig. 4.16**. The voltammogram shows a cathodic peak, i_{pc} at about -798.5 mV and an anodic peak, i_{pa} at about +664.2 mV. The cathodic peak corresponds to the reduction of Cd(II) to Cd(0) species while the anodic peak involves the process of oxidation from Cd(0) to Cd(II).

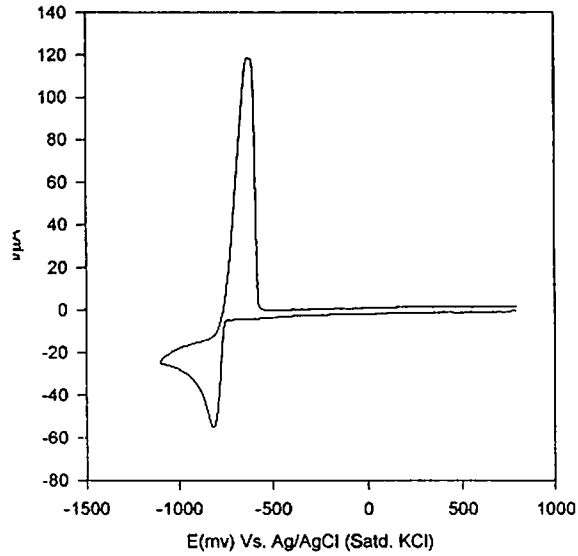

Fig. 4.16 Cyclic voltammogram of 1 mM Cd(II) in 0.1 M KCl solution at a scan rate of 100 mVs^{-1}.

The voltammograms of Cd(II) solution in 0.1 M KCl solution at different scan rates is shown in Fig. 4.17 and their respective peak currents and peak potentials are given in **Table 4.7(a)** and **4.7(b)**.

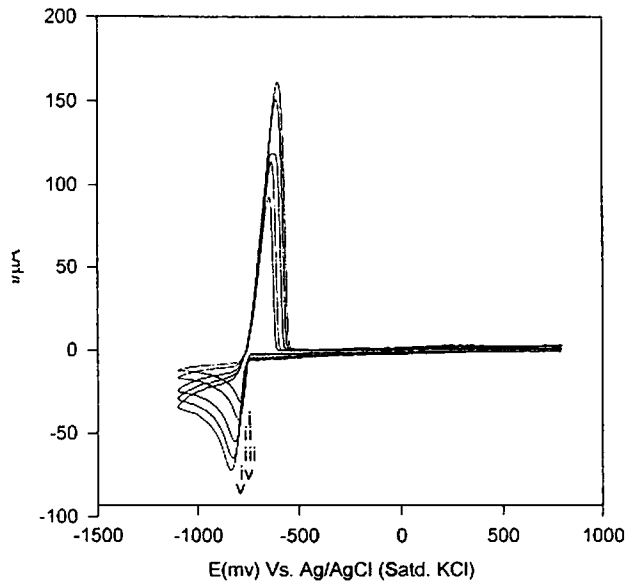

Fig. 4.17 Cyclic voltammogram of 1 mM Cd(II) in 0.1 M KCl solution at various scan rates (i) 25, (ii) 50, (iii) 100, (iv) 150 and (v) 200 mVs^{-1}.

Table 4.7(a): Current-Potential data of 1 mM Cd(II) in 0.1 M KCl at different scan rates.

Scan Rate (mVs^{-1})	Anodic Peak Current, i_{pa} (+)(μA)	Cathodic Peak Current, i_{pc} (-) (μA)	Anodic Peak Potential, E_{pa} (-)(mV)	Cathodic Peak Potential, E_{pc} (-)(mV)
25	89.16	26.67	694.03	778.51
50	110.90	37.57	656.72	798.41
100	126.18	45.51	664.18	815.38
150	149.08	51.72	649.25	828.36
200	159.27	57.41	634.33	835.82

Table 4.7(b): Derived parameters obtained from current-potential data.

Scan Rate (mVs^{-1})	$\Delta E = E_{pa} - E_{pc}$ (mV)	i_{pa}/ i_{pc}	$i_{pc}/ v^{1/2}$ (μAs^{-1})	$k_f \times 10^{-4}$
25	1472.54	3.34	5.33	19.14
50	1455.13	2.95	5.31	26.49
100	1479.56	2.77	4.55	32.43
150	1477.61	2.88	4.22	36.73
200	1470.15	2.77	4.06	41.21

At lower scan rate the peak current ratio i_{pa}/i_{pc} is equal to one, indicated that the redox couple Cd(II)/Cd(0) is reversible. However, away from reversibility becomes greater and greater with higher scan rates. This happens because increasing the scan rate is equivalent to increasing the rate of diffusion of the reduced material from the electrode **(Fig. 4.18)**. As a consequence, the diffusion process competes with the back electron transfer.

An interesting feature is that the i_{pa}/i_{pc} values also increases with increase in scan rates. The current function ($ip/v^{1/2}$) also decreases in the increase in scan rate but increases with increase in concentration. All of these criteria indicates that more than one electron involved in the redox process of Cd(II) and is not entirely a diffusion controlled process.

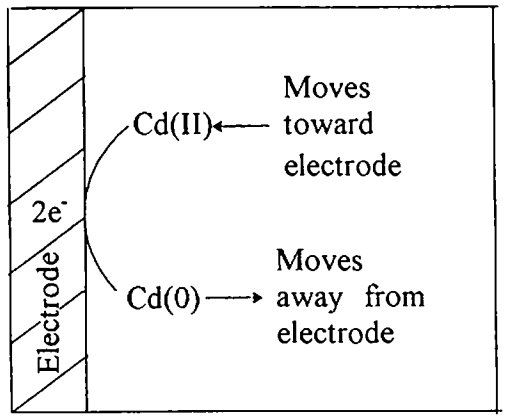

Fig. 4.18 Schematic diagram showing (a) transport of Cd(II) toward the electrode and Cd(0) away from the electrode following the reduction of Cd(II).

However, the variation of peaks currents with square root of scan rate ($\nu^{1/2}$) is linear, shown in **Fig. 4.19**.

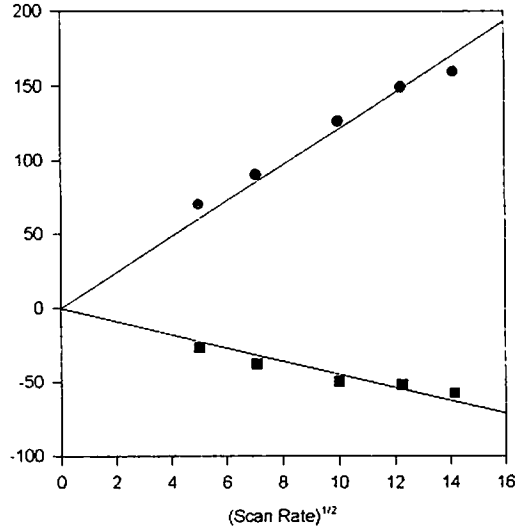

Fig. 4.19 Plots of peak current, i_p vs. square root of scan rate, $\nu^{1/2}$ for Cd(II).

Cyclic voltammograms of Cd(II) at different concentrations (0.2, 0.4, 0.6, 0.8 and 1 mM) in 0.1 KCl at a scan rate of 100 mVs^{-1} are also studied (**Fig. 4.20**) and their corresponding current and potential values are gathered in **Table 4.8(a)** and **4.8(b)**.

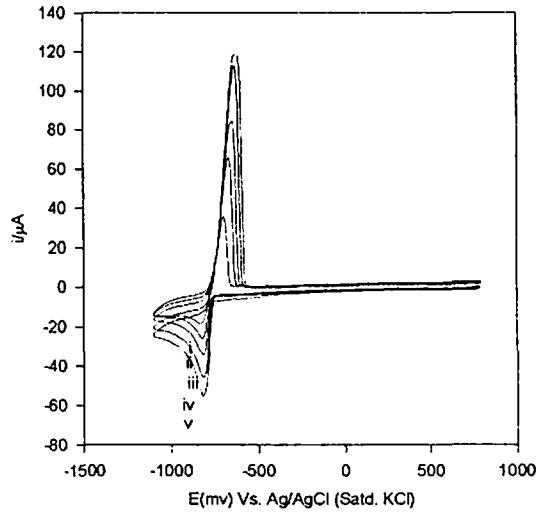

Fig. 4.20 Cyclic voltammogram of 1 mM Cd(II) in 0.1 M KCl at concentrations (i) 0.2, (ii) 0.4, (iii) 0.6, (iv) 0.8 and (v) 1 mM at 100 mVs^{-1} scan rate.

Table 4.8(a) Current-Potential data of 1 mM Cd(II) in 0.1 M KCl solution at different concentrations.

Concentrations (mM)	Anodic Peak Current, i_{pa} (+)(μA)	Cathodic Peak Current, i_{pc} (-)(μA)	Anodic Peak Potential, E_{pa} (-)(mV)	Cathodic Peak Potential, E_{pc} (-)(mV)
0.2	39.59	11.25	768.66	843.28
0.4	69.09	19.64	686.57	820.90
0.6	86.67	26.67	656.72	813.43
0.8	111.18	37.65	664.18	813.43
1.0	129.30	43.99	664.18	813.43

Table 4.8(b) Derived parameters obtained from current-potential data.

Concentrations (mM)	$\Delta E = E_{pa} - E_{pc}$ (mV)	i_{pa}/ ip_c	$i_{pc}/ \nu^{1/2}$ (μAs^{-1})
0.2	1611.94	3.52	1.13
0.4	1507.46	3.52	1.96
0.6	1470.15	3.25	2.67
0.8	1477.61	2.95	3.76
1.0	1477.61	2.94	4.40

The CVs of Cd(II) displays the following characteristics:

(i) Both reductive and oxidative current corresponds to a two-electron process at scan rates up to 200 mVs^{-1} at room temperature.

Cathodic peak, i_{pc}: $Cd(II) + 2e^- = Cd(0)$

Anodic peak, i_{pa}: $Cd(0) - 2e^- = Cd(II)$

(ii) Both the observed waves are reversible.

(iii) When the switching potential is 1.1 V, the electron transfer process is diffusion controlled.

4.1.5Cyclic Voltammetry of Cd(II) in Presence of Catechol at GCE

The electrochemical behavior of Cd(II) in presence of catechol in 0.1 KCl at pH 4.23 at room temperature has been studied using cyclic voltammetry. The voltammogram of Cd(II)–catechol in 0.1 M KCl at a scan rate of 100 mVs^{-1} is shown in **Fig. 4.21.** With catechol two cathodic peaks are found in the voltammogram at +187.5 and -839.3 mV whereas free Cd(II) shows only one cathodic peak at -798.5 mV. Peaks are shifted (for free catechol at 52.9 mV and free Cd(II) at +798.5). The peak responsible for Cd(II) reduction moves towards negative potential about 40 mV, an indication of hindering the reduction of Cd(II) to Cd(0) at least to a limit. This is expected that Cd(II), because of its positive charge, participates more readily and strongly in complexation with catechol than that of Cd(0). Similar situation is observed in the reverse scan.

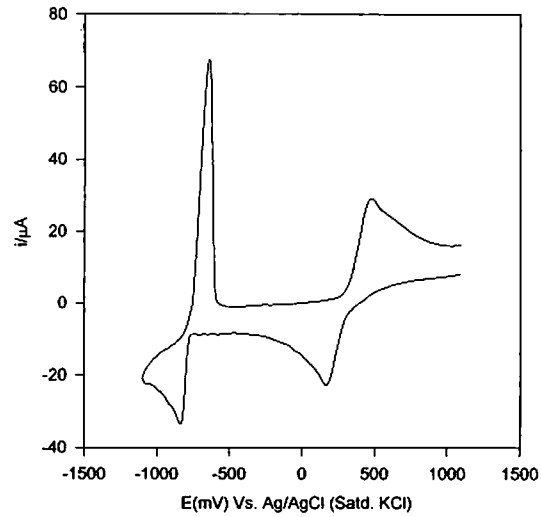

Fig. 4.21 Cyclic voltammogram of Cd(II)-Catechol (1:1 molar ratio) in 0.1 M KCl at 100 mVs^{-1} scan rate.

Fig. 4.22 and **4.23** show the comparison; the voltammograms of Cd(II)-catechol and catechol solution in 0.1 M KCl, and Cd(II)-catechol and Cd(II) in 0.1 M KCl solution.

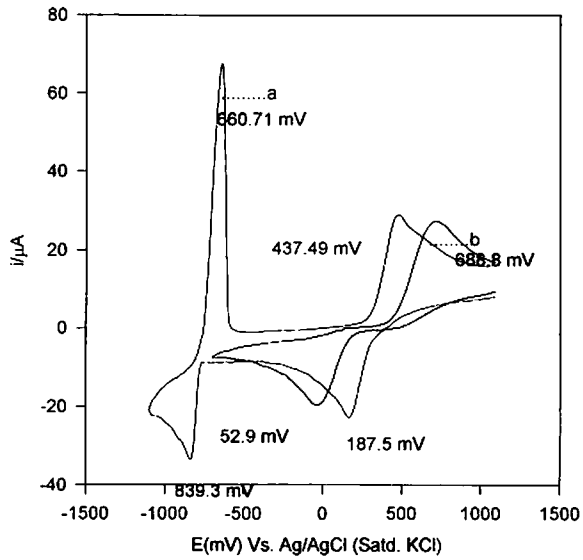

Fig. 4.22 Cyclic voltammogram of (a) Cd(II)-Catechol (1:1 molar ratio) and (b) 1 mM Catechol in 0.1 M KCl at 100 mVs^{-1} scan rate.

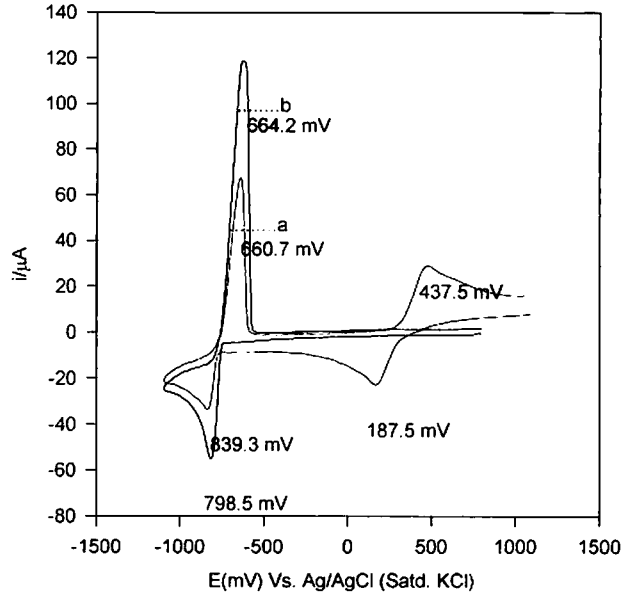

Fig. 4.23 Cyclic voltammogram of (a) Cd(II)-Catechol (1:1 molar ratio) and (b) 1 mM Cd(II) in 0.1 M KCl at 100 mVs^{-1} scan rate.

However, the low shifting of peak currents demonstrates that the metallic behavior of Cd(II) is prominent and does not participate in bonding with catechol as strong as Cu(II). The cyclic voltammogram of Cd(II)-catechol in 0.1 M KCl solution at different scan rates are also investigated (**Fig. 4.24**) and there are summarized in **Table 4.9(a)** and **4.9(b)**.

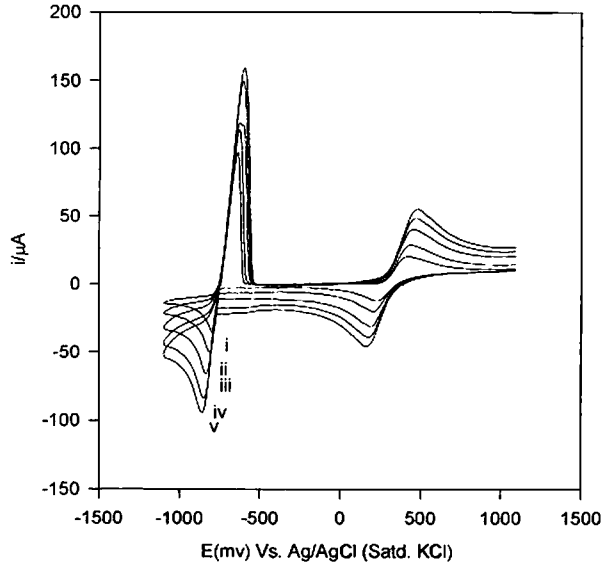

Fig. 4.24 Cyclic voltammograms of Cd(II)-Catechol in 0.1 M KCl at various scan rates (i) 25, (ii) 50, (iii) 100, (iv) 150 and (v) 200 mVs^{-1}.

Table 4.9(a) Current-Potential data of 1 mM Cd(II)-Catechol in 0.1 M KCl at different scan rates.

Scan Rate (mVs^{-1})	Anodic Peak Current, i_{pa} (μA)		Cathodic Peak Current, i_{pc} (μA)		Anodic Peak Potential, E_{pa} (mV)		Cathodic Peak Potential, E_{pc} (mV)	
	1 (+)	2 (+)	1 (-)	2 (-)	1 (+)	2 (-)	1 (+)	2 (-)
25	12.44	40.21	7.32	11.22	401.78	741.07	205.35	803.57
50	18.91	55.23	11.64	14.55	419.64	669.64	195.50	821.43
100	25.45	79.24	20.36	22.54	437.49	660.71	187.50	839.28
150	28.29	87.80	23.90	23.41	446.43	660.71	160.71	845.28
200	32.19	96.10	26.39	25.37	428.57	642.86	142.86	857.14

Table 4.9(b) Derived parameters obtained from current-potential data.

Scan Rate (mVs^{-1})	$\Delta E = E_{pa} - E_{pc}$ (mV)		i_{pa}/ i_{pc}		$i_{pc}/ v^{1/2}$ (μAs^{-1})		$k_f \times 10^{-4}$	
	1	2	1	2	1	2	1	2
25	196.42	62.50	1.70	4.40	1.46	2.24	5.27	7.94
50	224.14	151.79	1.63	4.50	1.60	2.06	8.13	10.23
100	250.00	178.57	1.25	3.52	2.04	2.25	14.49	15.96
150	285.72	184.57	1.18	3.75	1.95	1.91	17.02	16.59
200	285.14	214.28	1.22	3.79	1.86	1.80	18.79	18.24

The linearity between the current vs. the square root of scan rate is shown in Fig. 4.25. Cyclic voltammograms of Cu-Catechol at various concentrations (0.2, 0.4, 0.6, 0.8 and 1 mM) solution in 0.1 M KCl are also studied. Their results are depicted in Fig. 4.26 and current-potential values are tabulated in 4.10(a) and 4.10(b). The molar ratio of Cd(II) to catechol was varied from 1:1 to 1:2 and to 1:3 and their voltammograms are recorded. Only the observable difference is the cathodic current (i_{pc}) decreases and the anodic current increases with the increase of catechol concentration. That is, a complexation

reaction between Cd(II) and catechol occurs in the experimental condition. This reaction removes the oxidized form from solution as it is produced near the electrode.

$Cd(I) - e^- = Cd(II)$

$Cd(II) + Cat \rightarrow Cd(II)\text{-}Cat$

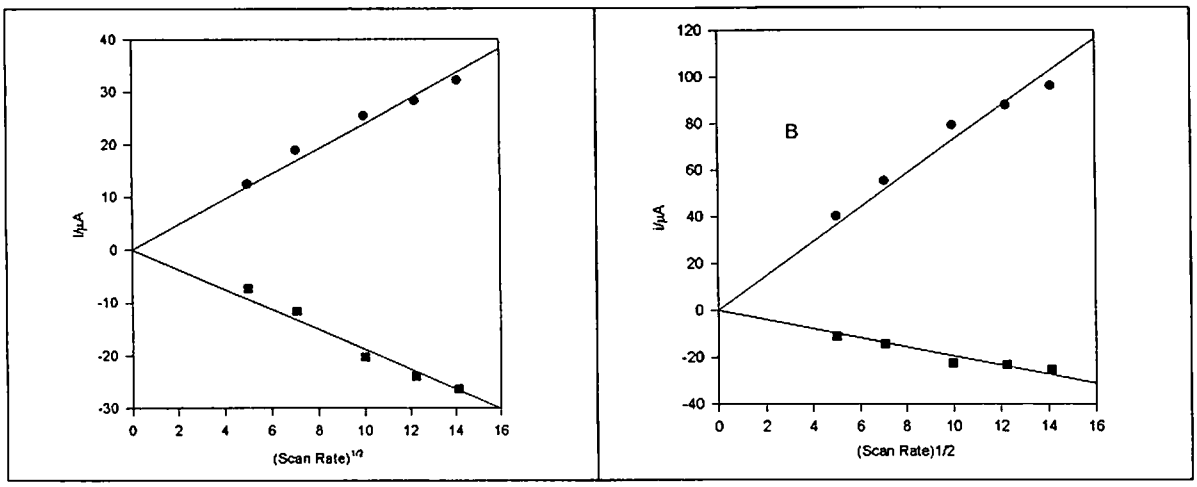

Fig. 4.25 Plots of peak current, i_p vs. square root of scan rate, $\nu^{1/2}$ for Cd(II)-Catechol; (A) i_{pa1} and i_{pc1} vs. $\nu^{1/2}$ and (B) i_{pa2} and i_{pc2} vs. $\nu^{1/2}$.

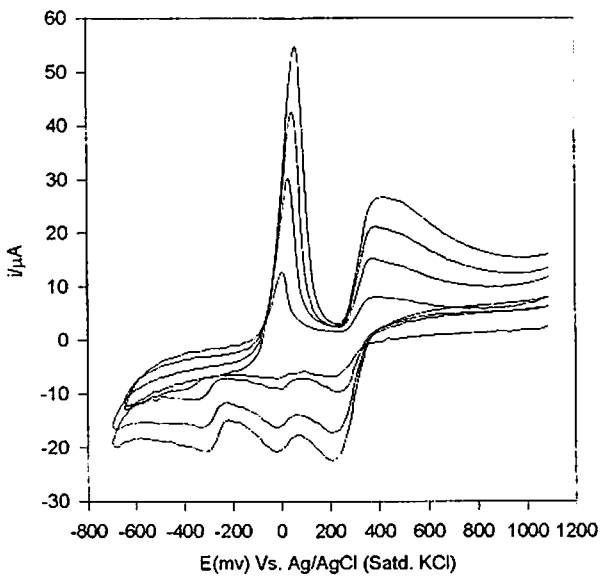

Fig. 4.26 Cyclic voltammograms of Cd(II)-Catechol at various concentrations (0.2, 0.4, 0.6, 0.8 and 1 mM) in 0.1 M KCl at 100 mVs^{-1} scan rate.

Table 4.10(a) Current-Potential data of Cd(II)-Catechol in 0.1 M KCl at different concentrations.

Conc. (mM)	Anodic Peak Current, i_{pa} (μA)		Cathodic Peak Current, i_{pc} (μA)		Anodic Peak Potential, E_{pa} (mV)		Cathodic Peak Potential, E_{pc} (mV)	
	1 (+)	2 (+)	1 (-)	2 (-)	1 (+)	2 (-)	1 (+)	2 (-)
0.2	7.2	33.6	6.8	9.8	392.9	741.1	187.5	848.2
0.4	12.9	55.7	11.4	14.6	428.6	678.6	187.5	839.3
0.6	18.4	57.1	12.7	15.4	428.6	696.4	178.6	839.3
0.8	18.9	60.1	15.1	15.9	428.6	714.3	178.6	839.3
1.0	25.4	79.2	20.4	22.5	437.5	660.7	187.5	839.3

Table 4.10(b) Derived parameters obtained from current-potential data.

Conc. (mM)	$\Delta E = E_{pa} - E_{pc}$ (mV)		i_{pa}/ i_{pc}		$i_{pc}/ \nu^{1/2}$ (μAs^{-1})	
	1	2	1	2	1	2
0.2	580.35	1589.28	1.06	3.43	0.68	0.98
0.4	616.07	1517.85	1.14	3.81	1.14	1.46
0.6	607.14	1535.71	1.45	3.70	1.27	1.54
0.8	607.14	1553.57	1.25	3.76	1.51	1.60
1.0	625.00	1500.00	1.25	3.52	2.04	2.25

Thermodynamic and kinetic parameters of all the studied systems are calculated. The parameters obtained for different system only at 1 mM concentration and at 100 mVs^{-1} scan rate are shown in **Table 4.11.**

Table 4.11 Calculated thermodynamic and kinetic parameters for different systems at 1 mM concentration and at 100 mVs^{-1} scan rate.

Systems	αn_a			b			D x 10^{-5}			k_f x 10^{-4}		
	1	2	3	1	2	3	1	2	3	1	2	3
Catechol	0.1264	-	-	0.468	-	-	9.45	-	-	23.28	-	-
Cu(II)	0.382	0.787	-	0.155	0.075	-	1.22	0.282	-	14.45	1.00	-
Cu-Catechol	0.311	1.04	0.433	0.190	0.057	0.1366	8.66	0.108	0.279	34.98	7.08	7.7
Cd(II)	0.403	-	-	0.147	-	-	5.75	-	-	32.43	-	-
Cd-Catechol	0.149	0.867	-	0.396	0.068	-	3.10	0.66	-	14.49	15.96	-

4.2 Chronocoulometric (CC) study of Different System

Double potential step chronocoulometric experiments were performed for 1 mM catechol, Cu(II), Cd(II), and 1:1 mixtures of Cu-catechol and Cd-catechol systems and the resulting chronocoulograms were represents in Figs. 4.27 and 4.28. A separate chronocoulogram for the supporting electrolyte was performed to obtain the background change. The background change for the double layer was recorded as 10 μC (Fig. 4.28). The Q_{total} for the catechol, and Cu(II) system was recorded ~35 μC and ~113 μC respectively. On the other hand, the Q_{total} for the Cu(II)-catechol system was ~160 μC. Elimination of the charge for double layer, Q_{dl} (=10 μC) results into ~150 μC charge, obtained for the complex. Therefore, this equivalent mass of the Cu-catechol complex was formed in this condition. Similarly, for Cd-catechol ~130 μC charge was produced for the combination of 1:1 molar ratio of Cd(II) and catechol system. CC study also shows a strong indication of complexation between Cu and catechol and Cd and catechol.

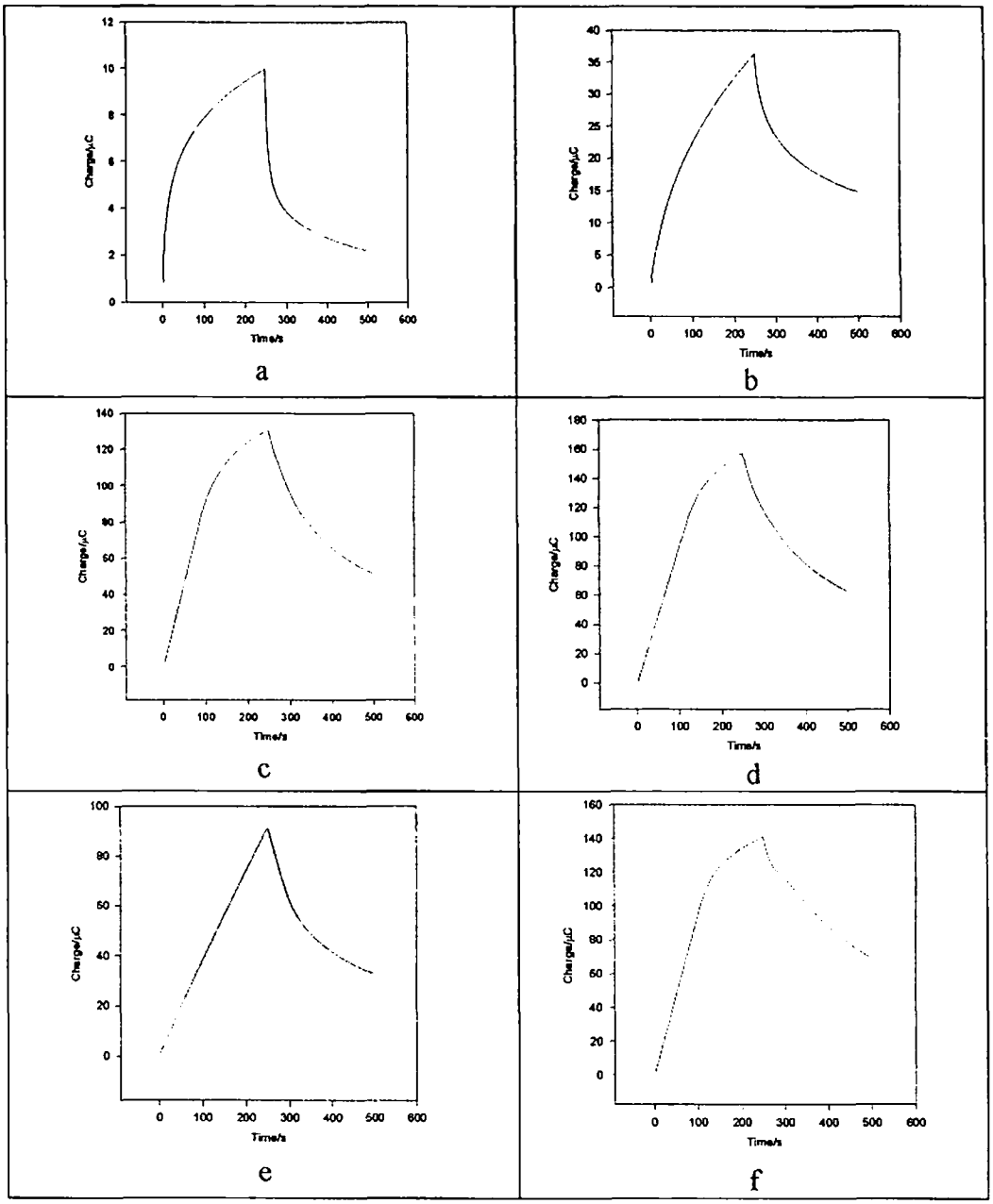

Fig.4.27 Chronocoulograms of (a) 0.1 M KCl, (b) 1 mM Catechol, (c) 1 mM Cu(II), (d) Cu-Catechol (1:1 molar ratio), (e) 1 mM Cd(II), and (f) Cd-Catechol (1:1 molar ratio).

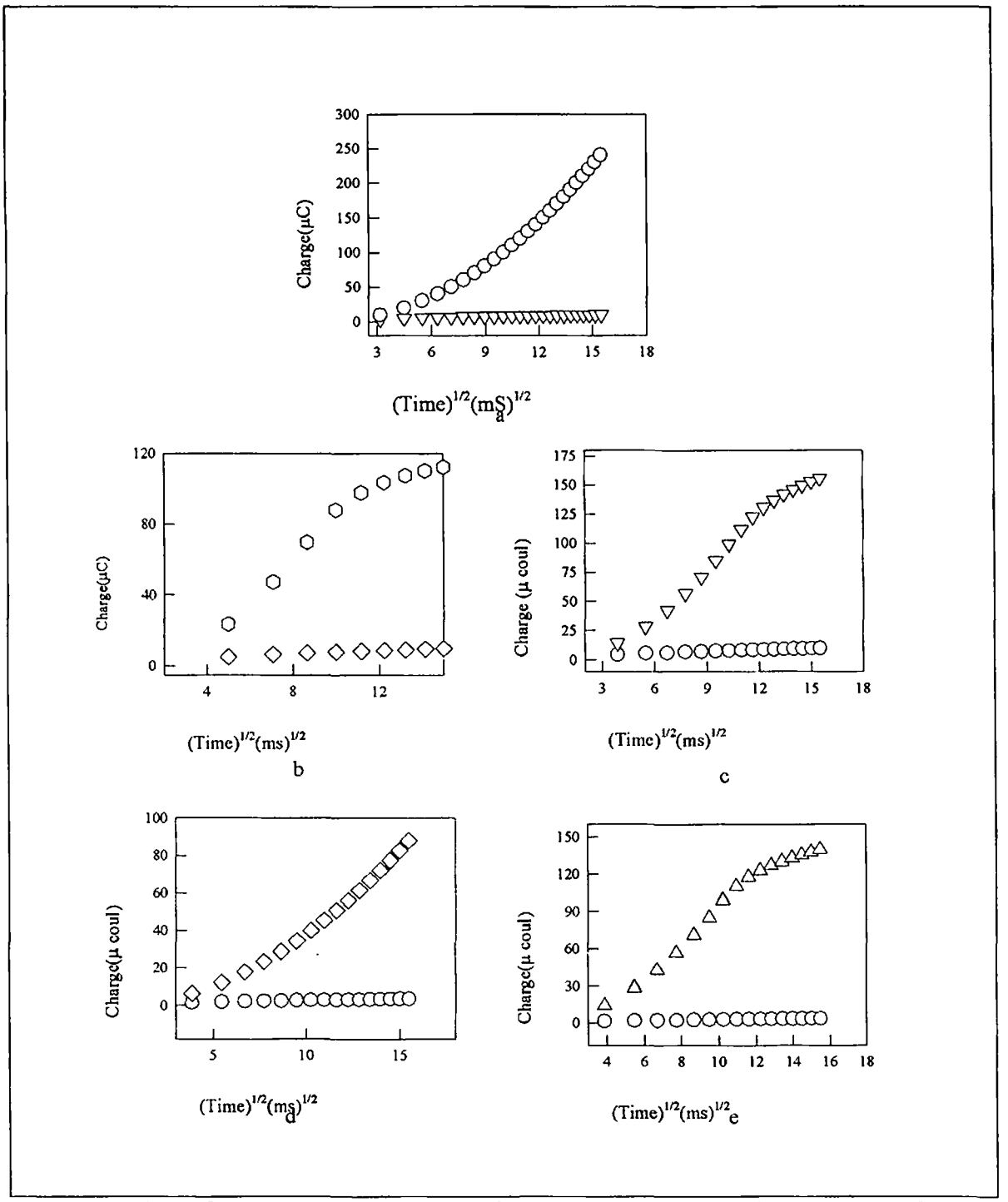

Fig. 4.28 Plots of charge vs. square root of time for (a) 1 mM Catechol, (b) 1 mM Cu(II), (c) Cu-Catechol (1:1 molar ratio), (d) 1 mM Cd(II), and (e) Cd-Catechol (1:1 molar ratio).

For further information of complexation between metals (Cu, and Cd) and catechol, heterogeneous electron-transfer rate constants from chronocoulometric data for the different systems have been calculated according to the theory described in chapter 1. The value of the heterogeneous electron-transfer rate constants have been compiled in **Table 4.12**.

Table 4.12: k_f – values obtained from CC study for different systems.

Systems	$t_i^{1/2}$	Tafel slope	k_f(cm/s)$\times 10^3$
Catechol	3.0	2.4838	0.1626
Cu(II)	3.0	7.904	0.517
Cu-catechol	2.8	12.4112	0.871
Cd(II)	4.2	6.4712	0.303
Cd-catechol	3.5	11.1317	0.626

4.3 Spectrophotometric Study of Cu(II)-Catechol and Cd(II)-Catechol

The composition of Cu(II)-catechol and Cd(II)-catechol complex under similar experimental conditions, at which cyclic voltammetric studies were performed, was studied using spectrophotometric method. This method helps us to establish

(i) Whether the interaction between Cu(II) and Cd(II) with catechol in aqueous medium at pH 4.32 occurs,

(ii) If happens, what would be its compositional ratio,

(iii) And a support to our cyclic voltammetric observation that both metal ions form complex with catechol.

4.3.1 Composition of Metal(Cu(II) and Cd(II))-Catechol Complex

A series of solutions was prepared, each containing the same total number of moles of metal (= Cu(II) or Cd(II)) and catechol, but a different ratio.

The ratio was systematically varied from large to small, and measures the absorbance at wavelength 222 nm in each solution. Plots of absorbance difference versus mole fraction of catechol of each solution gave V shaped graphs (Fig.4.29(a) and 4.29(b)), and the stoichiometry of catechol complexes of Cu(II) and Cd(II) was extracted.

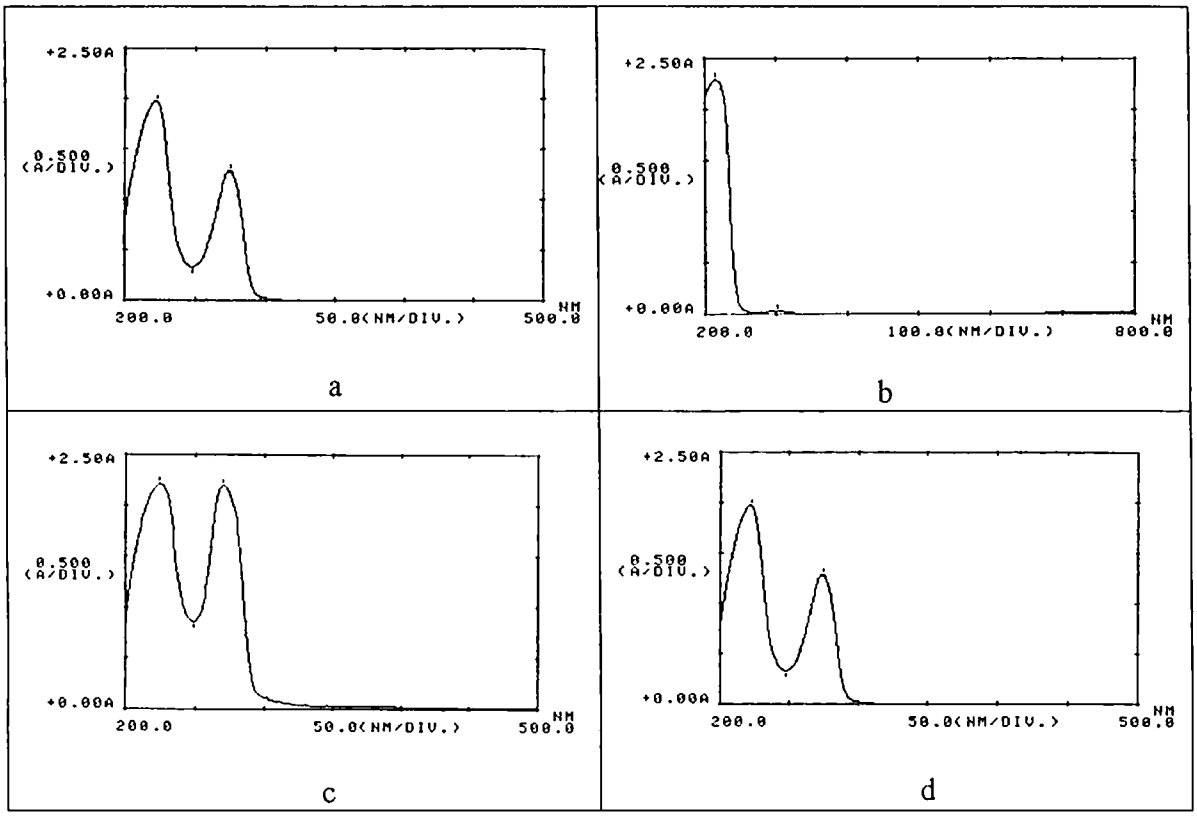

UV spectra of (a) catechol, (b) Cu(II), (c) 1:1 mixture of catechol with Cu(II) and (d) 1:1 mixture of catechol with Cd(II) at pH 4.23.

In both cases, the intersection in the plot occurs at moles catechol = 0.5/(1.0 - 0.5) = 1. Therefore, the stoichiometry of catechol complexes of Cu(II) and Cd(II) is 1:1 having the possible geometry in the solution phase.

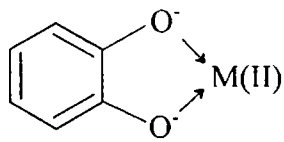

where M(II) = Cu(II) or Cd(II).

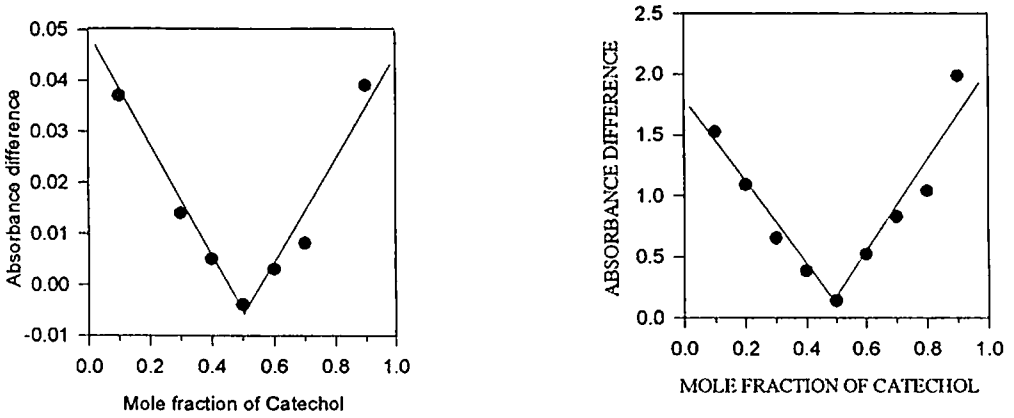

Fig. 4.29 Plots of absorbance differences *vs.* mole fraction of Catechol for (a) Cu(II)-Catechol, and (b) Cd(II)-Catechol systems.

Table 4.13 Absorbance values for Cu(II) and Catechol system at pH 4.23 for Job's method.

[Catechol] x 10^4 mM	[Cu(II)] x 10^4 mM	Absorbance of Catechol, (A_L)	Absorbance of Cu(II), (A_M)	Absorbance of Cu(II) + Catechol, (A_{ML})	Absorbance Difference, $A_D = A_{ML} - (A_M + A_L)$
1	9	0.541	2.192	2.258	-0.475
2	8	1.037	2.166	2.293	-0.91
3	7	1.530	2.089	2.272	-1.347
4	6	1.861	2.000	2.244	-1.617
5	5	2.092	1.986	2.217	-1.861
6	4	2.146	1.574	2.241	-1.479
7	3	2.163	1.240	2.231	-1.172
8	2	2.184	1.035	2.258	-0.961
9	1	2.242	0.013	2.238	-0.017

Table 4.14 Absorbance values for Cd(II) and Catechol system at pH 4.23 for Job's method.

[Catechol] x 10^4 mM	[Cd(II)] x 10^4 mM	Absorbance of Catechol, (A_L)	Absorbance of Cd(II), (A_M)	Absorbance of Cd(II) + Catechol, (A_{ML})	Absorbance Difference, $A_D = A_{ML} - (A_M+A_L)$
1	9	0.541	0.00	0.588	0.047
2	8	0.000	0.00	0.000	0.000
3	7	1.530	0.00	1.544	0.014
4	6	1.861	0.00	1.866	0.005
5	5	2.092	0.00	2.088	-0.004
6	4	2.146	0.00	2.149	0.003
7	3	2.163	0.00	2.173	0.010
8	2	0.000	0.00	0.000	0.000
9	1	2.348	0.00	2.387	0.039

5. Summary And Conclusions

Interaction of divalent metal ions such as Cu(Il) and Cd(II) with Catechol has been studied by cyclic votammetric and chronocoulometric technique at a glassy carbon electrode (GCE). Cyclic volatammograms of free metal ions and in presence of catechol are recorded in their aqueous and in 0.1 M KCl solution. The speciation of the Cu-Catechol and Cd-Catechol complexes were studied and established by cyclic voltammetric and chronocoulometric techniques. The stoichiometry of the complexes were established by Job's method using UV-visible spectroscopy. It was found that cadmium and copper both form 1:1 complexes with catechol.

The following conclusions can be drawn for the electrochemical study of Copper-Catechol and Cadmium-Catechol complex systems in acidic aqueous media.

1) Catechol shows two steps processes of which each step involving one-electron transfer and overall two-electron redox process. The quinone product of the two-electron oxidation of catechol is stable on the cyclic voltammetric time-scale. Evidence of the prominent adsorption of quinone product was found from cyclic voltammetric and chronocoulometric data.

2) Two one-electron transfer processes are observed in the CV of Copper(II), of which the Cu(Il)/Cu(I) couple is reversible and the Cu(I)/Cu(0) is quasi-reversible. However, in presence of Catechol, both anodic and cathodic peaks are shifted, that demonstrates the formation of complex between Copper and Catechol in solution. The nature of voltammograms at different metal to Catechol ratios also supports our observation.

3) In cyclic voltammetric studies of cadmium system, one-step two electron transfer process was observed in CV, of which the Cd(II)/Cd(0) couple is quasi-reversible. In presence of Catechol, shifting of both anodic and cathodic peaks occurs possibly due to the formation of coordination complex between Cd(II) and Catechol under the

experimental conditions followed in this studies. Gradual decrease of cathodic current with the increase of Catechol concentration also demonstrates the Cadmium-Catechol interaction.

4) To confirm the complexation reactions of Cu(II) and Cd(II) with Catechol, diffusion coefficients of the metals in the presence and absence of Catechol was calculated. It was found that Catechol is readily diffused in the electrical layer whether the diffusion rate of the complex is slower. The heterogeneous electron-transfer rate constant is highly influenced by these values of the diffusion co-efficient. The combined effects of the electro-active materials catechol and copper make the copper-catechol complex highly electroactive. Therefore, the electron-transfer of Copper-catechol from the electrode to the diffused layer is faster than bare catechol and copper. In the case of Cadmium-Catechol complex the electron transfer rate is slower than bare catechol and cadmium.

5) Chronocoulometric studies of the neutral metal ions and their complexes under the same experimental conditions confirmed the formation of the Cu-Catechol and Cd-Catechol complex. The heterogeneous electron-transfer rate constant was also calculated from chronocoulometric data. These data also support the above results and indicate the formation of complexes of Cupper and Cadmium with Catechol.

6) UV-Visible spectroscopic studies (Job's method) at different mole ratios of the metal ions (Cu^{2+} and Cd^{2+}) and the ligand (Catechol) shows that Cu^{2+} and Cd^{2+} ions form 1:1 complexes with catechol respectively.

References

1. J. O. Nriagu, and J. M. Pacyna, *Nature*, **333**, 147, 1989.
2. *"Chemistry, Toxicity, and Bioavailability of Copper and Its Relationship to Regulation in the Marine Environment"*, The workshop report, San Diego, CA, June 3 - 4, 1997.
3. R. P. Naidu, N. J. de Lacy Rengasamy, and B. A. Zarcinas, *"Soil Solution Composition of Some Sodic Soils"*, pp. 155 –161, 1995.
4. M. J. McLaughlin, K.G. Tiller, and M. K. Smart, *Aust. J. Soil Res.*, **35**, 183 -198, 1997.
5. M. J. McLaughlin, L. T. Palmer, K. G. Tiller, T. A. Beech, and M. K. Smart, *J. Environ. Qual.*, **23**,1013–1018, 1994.
6. J. Garcia-Miragaya, and A. L. Page, *Soil Sci. Soc. Am. J.*, **40**, 658–663, 1976.
7. R. S. Nicholson, and I. Shain, *Anal. Chem.*, **36**, 706, 1964.
8. W. Devries, and E. Van Delen, *J. Electroanal. Chem.*, **6**, 490, 1963.
9. J. C. Bokros, *Carbon*, **15**, 355, 1977.
10. R. C. Engstrom, *Anal. Chem.*, **56**, 890, 1984.
11. D. Fagan, I. Hu, and T. Kuwana, *Anal. Chem.*, **57**, 2759, 1985.
12. G. G. Wallace, *Trends Anal. Chem.*, **4**, 145, 1985.
13. C. K. Mann, in A. J. Bard, Ed., *"Electroanalytical Chemistry"*, Marcel Dekker, New York, Vol. **3**, p. 57, 1969.
14. J. Wang, *"Analytical Chemistry"*, 2nd Ed., Wiley-VCH, p. 103, 2000.
15. J. N. Gaur, and M. M. Palrecha, *J. Electroanal. Chem.*, 15, 583, 1968.
16. B. W. Rossiter, and J. F. Hamilton, *"Physical Methods of Chemistry, Electrochemical Methods"*, John Willey & Sons Inc., Vol. **II**, Chapter-1, 1986.
17. B. W. Rossiter, and J. F. Hamilton, *"Physical Methods of Chemistry, Electrochemical Methods"*, John Willey & Sons Inc., Vol. **II**, Chapter-5, 1986.
18. F. C. Anson, *Anal. Chem.*, **38**, 54, 1966.
19. J. H. Christie, R. A. Osteryoung, and F. C. Anson, *J. Electroanal. Chem.*, **13**, 236, 1967.
20. F. C. Anson, and R. A. Osteryoung, *J. Chem. Educ.*, **60**, 293, 1983.
21. J. H. Christie, R. A. Osteryoung, and F. C. Anson, *J. Electroanal. Chem.*, **13**, 347, 1967.
22. F. C. Anson, J. H. Christie, and R. A. Osteryoung, *J. Electroanal. Chem.*, **13**, 343, 1967.
23. A. J. Bard, and L. R. Faulkner, *"Electrochemical Methods"*, Willey, New York, pp. 199-206, 1980.
24. P. T. Kissinger, and W. R. Heinman, *"Laboratory Techniques in Electroanalytical*

Chemistry", Marcel Dekker Inc. New York, p. 51, 1996.
25. P. Delahay, *"New Instrumental Methods in Electrochemistry"*, Interscience, New York, 1954.
26. J. H. Christie, *J. Electroanal. Chem.*, **13**, 79, 1967.
27. J. H. Christie, G. Lawer, R. A. Osteryoung and F. C. Anson, *Anal. Chem.*, **35**, 1979, 1963.
28. F. C. Anson, *Anal. Chem.*, **38**, 55, 1966.
29. J. H. Christie, R. A. Osteryoung, and F. C. Anson, *Anal. Chem.*, **13**, 236, 1967.
30. C. M. Elliott, and R. W. Murray, Anal. Chem., **47**, 908, 1975.
31. T. Kambara, *Bull Chem. Soc., Japan*, **27**, 527, 1954.
32. A. J. Bard, and L. R. Faulkner, *"Electrochemical Methods: Fundamentals and Applications"*, John Willey & Sons, New York, pp. 132, 142-143, 1980.
33. D. J. Barclay, and F. C. Anson, *J. Electrochem. Soc.*, **116**, 438, 1969.
34. P. T. Kissinger, *Current Separations*, **6(4)**, 62, 1985.
35. A. K. Srivastava, and P. C. Jain, *"Chemical Analysis – An Instrumental Approach"*, S. Chand & Company Ltd., Ram Nagar, New Delhi, p. 238, 1997.
36. R. Panico, and W. H. Powell, (Eds.), *A Guide to IUPAC Nomenclature of Organic Compounds 1993*, Oxford: Blackwell Science, 1994.
37. M. R. G. Pereira, *J. Bras. Patol. Med. Lab.*, **40**, 280-285, 2004.
38. W. L. C. Almeida, D. N. Vitor, M. R. G. Pereira, D. S. de Sá, L. D. G. Alvarez, A. M. Pinheiro, S. L. Costa, M. F. D. Costa, Z. N. Rocha, R. S. El-Bachá, *J. Chil. Chem. Soc.*, **52(3)**, 1240-1243, 2007.
39. D. P. H. Laxen, and R. M. Harrison, *Water Res.*, **1**, 11, 1977.
40. C. J. M. Kramer, and J. C. Duinker (Eds.), *"Complexation of Trace Metals in Natural Waters"*, 1984.
41. R. F. C. Mantoura, *"Marine Organic Chemistry"*, Elsevier, Amsterdam, pp. 179-223, 1983.
42. C. L. Chakraboarti, Lu Yanjia, and J. Cherg. *Anal. Chim. Acta*, **47**, 264, 1993.
43. F. Banda, and J. Kouba, *Bull. Environ. Contan. Toxicology*, **46**, 466, 1991.
44. C. M. G. Van den Berg, *Anal. Proc.*, **28**, 581, 1991.
45. J. R. Scroft, and R. Gardner, *Anal. Proc.*, **28**, 61, 1991.
46. H. Van, and P. Lecuwen, *Anal. Proc.*, **28**, 67, 1991.
47. D. M. J. Tubbing, W. Admiraal, R. F. M. J. Clever, M. Iqbal, D. Van de Meent, and W. Verweij, *Water Res.*, **28(1)**, 37, 1994.
48. C. M. G. Van de Berg, A. G. Merks, and E. K. Dursma, *Esturarine Lonstal Shelf. Sci.*, **24**, 785, 1987.
49. G. M. Morrisn, and Wei Chen, *Anal. Proc.*, 28, 1991.
50. G. M. Morrison, E. Batlcy, T. M. Florence, *Anal. Proc.*, 791, 1989.
51. F. M. Matysik, and G. Werner, *Analyst*, **118**, 1523, 1993.
52. H. P. Wu, *J. Anal. Chem.*, **68**, 1639, 1996.
53. D. P. H. Laxen, and R. M. Harrison, *Sci. Total Environ.*, **19**, 59, 1981.
54. D. M. J. Tubbing, W. Admiral, M. J. Cleven, D. Van de Meent, and W. Verweij,

Wat. Res., **28(1)**, 37, 1994.

55. W. R. Murphy, Jr., *"Ph. D. Dissertation"*, University of North Carolina at Chapel Hill, 1984.
56. A. J. Bard, and L. R. Faulkner, *"Electrochemical Method"*, Wiley, New York, pp. 290-291, 1975.
57. J. Q. Chambers, *"In the Chemistry of the Quinoid Compunds"*, Vol. **2**; S. Patai, and Z. Rappoport (Eds.), John Wiley & Sons, New York, pp. 719-756, 1988.
58. B. W. Rossiter, and J. E. Hamilton (Eds.), *"Physical Methods of Chemistry"*, Vol **II**, *"Electrochemical Methods"*, John Wiley & Sons Inc., USA, p. 311, 1986.